Hand-off Analysis for 5G Networks Using Poisson Point Process in Homogeneous and non-Homogeneous Environments

A thesis submitted toward partial fulfillment
of the requirements for the degree of

Master of Engineering in
Electronics & Tele-communication
Engineering

Submitted by
Indranil Halder
ROLL NO: **M4ETC22025**
REGISTRATION NO: **154094 OF 2020-21**

Under the guidance of
Prof. Iti Saha Misra

Department of Electronics &
Telecommunication Engineering
Jadavpur University
Kolkata-32

Course affiliated to
Faculty of Engineering and Technology
Jadavpur University
Kolkata-700032, India

Aug, 2022

M.E. (Electronics & Tele-communication Engineering) course affiliated to
Faculty of Engineering and Technology
Jadavpur University
Kolkata, India

CERTIFICATE OF RECOMMENDATION

This is to certify that the dissertation entitled "**Hand-off Analysis for 5G Networks Using Poisson Point Process in Homogeneous and non-Homogeneous Environments**" has been carried out by **INDRANIL HALDER (University Registration No: 154094 of 2020-2021)** under my guidance and supervision and be accepted in partial fulfillment of the requirements for the degree of Master of Engineering in Electronics & Tele-communication Engineering. The research results presented in the thesis have not been included in any other paper submitted for any degree to any other University or Institute.

Prof. Iti Saha Misra
(SUPERVISOR)

Department of Electronics &
Telecommunication Engineering
Jadavpur University
Kolkata-700032, India

Prof. Manotosh Biswas
(HEAD OF DEPARTMENT)

Department of Electronics &
Telecommunication Engineering
Jadavpur University
Kolkata-700032, India

Prof. Chandan Mazumdar
(DEAN)

Faculty of Engineering & Technology
Jadavpur University
Kolkata-700032, India

M.E. (Electronics & Tele-communication Engineering) course affiliated to
Faculty of Engineering and Technology
Jadavpur University
Kolkata, India

CERTIFICATE OF APPROVAL **

This foregoing thesis is hereby approved as a credible study of an engineering subject carried out and presented in a manner satisfactory to warrant its acceptance as a prerequisite to the degree for which it has been submitted. It is understood that by this approval the undersigned does not endorse or approve any statement made or opinion expressed or conclusion drawn therein but approves the thesis only for the purpose for which it has been submitted.

----------	**----------**
External Examiner	**Internal Examiner**

** Only in case the thesis is approved.

DECLARATION OF ORIGINALITY AND COMPLIANCE OF ACADEMIC ETHICS

I hereby declare that this thesis contains a literature survey and original research work by the undersigned candidate, as part of his **Master of Engineering in Electronics & Tele-communication Engineering** studies during academic session 2021- 2022.

All information in this document has been obtained and presented by academic rules and ethical conduct.

I also declare that, as required by this rules and conduct, I have fully cited and referred all material and results that are not original to this work.

Name: Indranil Halder

Exam roll number: M4ETC22025

Class roll number: 002010702025

Thesis title: **Hand-off Analysis for 5G Networks Using Poisson Point Process in Homogeneous and Non-Homogeneous Environments**

_____ _____

Signature Date

Acknowledgment

I am deeply indebted to my supervisor Prof. Iti Saha Misra for her valuable guidance, active supervision, and innovative ideas that make it possible to present this thesis paper. Her pieces of advice will help me in future research work. I am privileged to witness her enthusiastic and dedicated interest in advanced research that motivates me and enriches my growth as a student and a researcher.

Words cannot express my gratitude to my friends and seniors who constantly supported me and without their moral support, this thesis would have never been made possible. So, I convey my heartiest thanks to Arijeet Ghosh, Rakhi Mondal, and Urbi Basu for their generous assistance.

Additionally, I would like to thank the entire Department of Electronics and Telecommunication Engineering, and all the people, who directly and indirectly impacted and inspired me for writing the same.

Lastly, I would be remiss in not mentioning my family, especially my parents. Their belief in me has kept my spirits and motivation high during this process.

Place: Kolkata
Date: ----------
(Mr. Indranil Halder)
Department of
Electronics & Telecommunication Engineering
Jadavpur University

Abstract

Due to the high bandwidth of the 5G spectrum, the cell coverage area in 5G gets reduced promoting the Ultra-Dense Network (UDN) deployment. To keep user Quality of Service (QoS) intact, 5G needs to maintain an enormous number of active connections from Base Stations (BS) to mobile users during movement. Thus, in this thesis, we primarily show a process for the enhancement of network mobility in 5G by increasing the successful hand-off rate against one of the primary QoS parameters, Signal to Interference plus Noise Ratio (SINR). To construct mobility in simulation, we adopt user distribution as a spatially distributed Poisson Point Process (PPP) and iteratively deployed the same PPP to impose randomness in motion. The network models where PPP has been incorporated comprise three different case studies for analyzing the gradual enhancement of successful hand-off (in terms of successful Poisson arrival metric). Primary observations reveal that the successful handoff rate increases for higher SINR if we choose the interferer BSs layer as a group of selected cells forming variable cluster radius. Moreover, we found that the successful handoff percentage in higher SINR increases further by applying the Heterogeneous Network (HetNet) of two different network tiers. The first one is the traditional Femto Base Stations (FBSs) and the second is the Macro Base Stations (MBSs). Additional work has been made to establish a direct relationship between the average user rate and the Poisson arrival parameter λ and depicts how λ can be suitably varied to have control over the network load. Our work finally extends to the complex network environment where we have considered networks to be of anisotropic type. It is called a fractal coverage network where different paths in the network undergo different path loss exponents. It resembles a real-time network and performance analysis shows the behavior of coverage and association probability based on the SINR threshold in this multi-directional path loss model. It could be concluded that although the QoS of the 5G network can be taken care of through multiple techniques, it will still face a heavy network overload which is the key challenge in 5G UDN deployment.

Table of Contents

Abbreviations

5G	5th Generation
NR	New Radio
HO	Hand-Off / Hand-Over
CN	Core Network
RSS	Received Signal Strength
SINR	Signal to Interference Plus Noise Ratio
UDN	Ultra-Dense Network
BS	Base Station
MBS	Macro Base Station
FBS	Femto Base Station
HetNet	Heterogeneous Network
PPP	Poisson Point Process
UE	User Equipment
LOS	Line of Sight
NLOS	Non-Line of Sight
LTE	Long-Term Evolution
RSSI	Received Signal Strength Indicator
RSRP	Reference Signal Received power
TTT	Time to Trigger
LMM	Localized Mobility Management
LAS	Local Access Servers

LSC	Local Service Centre
LDC	Local Data Centre
PDU	Protocol Data unit
ABG	Alpha-Beta-Gamma
ISD	Inter-Site Distance
CSI	Channel State Information
HSS	Home Subscriber Server
EPC	Evolved Packet Core
MME	Mobility Management Entity
S-GW	Serving Gateway
RACH	Random Access Channel Transmission
RRC	Radio Resource Control
RAN	Radio Access Network
NF	Network Function
SMF	Session Management Function
UPF	User Plain Function
AMF	Access and Mobility Management Function
ITU	International Telecommunication Union
3GPP	3rd Generation Partnership Project
E-UTRAN	Evolved UMTS Terrestrial Radio Access Network

List of Tables

List of Figures

.

Chapter 1 Introduction

1.1 Introduction

In modern days, the requirement for huge data support for millions of users with a substantially higher data rate is achieved at higher frequencies in the 5th Generation (5G) technology standard [1]**.** The 5G NR (New Radio) air interface handles the exponentially increasing requirement, which is a new Radio Access Technology (RAT) of the 5G network, developed by 3GPP. The basic goal is to increase the network capacity by providing high bandwidth to 5G networks. The new technology standard along with the new radio bands have introduced FR1 as a sub 6 GHz band and FR2 as mm-wave) to drive the requirement of user capacity [2] sufficiently.

The term hand-off arises due to the movement of users between two base stations inside a network. It is crucial because it keeps a session active or connected while moving around [3] from one BS's coverage to another BS's coverage. It has a direct impact not only on the network service quality but on the network performance also. Conventional Hand-off is executed in a network by measuring the received signal strength indicator (RSSI) at the User Equipment (UE) end [4]. Though RSSI is the primary parameter to terminate and establish new connections, it is not alone sufficient to make a final hand-off decision because it does not guarantee the QoS expectation (like bandwidth efficiency, etc.) of the user [5]. Another parameter SINR thus comes into the picture (the ratio of signal and total interference and noise power) which plays an additional role to measure the channel quality in the network. Therefore, RSSI along with SINR, both the parameters become the

key hand-off metrics for successful hand-off evaluation.

To minimize redundant hand-offs which cause heavy signaling overhead [6], an extra parameter called, offset is introduced in 3GPP [4]. Here, hand-off is triggered when serving BS meets threshold as well as offset criteria while switching to target BS. However, this offset method is unsuitable for deploying highly dense BS in 5G because of the fast variation of the 5G channel quality. Additionally adding a new evaluation metric like offset, increases network latency resulting in huge network delays which are not at all desirable in an active 5G connection [7]. Therefore, to increase network performance, this paper's motto solely focuses on increasing the successful hand-off rate based on threshold criteria only.

On another note, the fractal behavior of the network on the account of the real-time propagation environment is also crucial for the decision of hand-off triggering. So, it becomes necessary to consider the anisotropic path loss models in complex scenarios for analyzing the performance of 5G ultra-dense networks [8]. The transmission link can be of LOS and NLOS types which depend on the characteristics of channels when subjected to different blockages. Due to its effect, the empirical path loss co-efficient changes from one region to another resulting in multidirectional path loss. For estimating the impact of anisotropic path loss in such a network, some of the parameters like SINR-based probability of coverage & achievable rate can be drafted in comparison to the isotropic path loss for a clear distinction between them. It shows a negative impact on coverage performance [9] than the uniform path loss. Contradicting the rule of assigning the highest SINR to the user as a part of target BS selection, the association probability in the complex fractal cells shows that an anisotropic network doesn’t guarantee the best fit hand-off performance all the time likewise an isotropic network.

1.2 Objective

The ultra-small cell deployment and 5G hand-off management together become an essential topic of research in today's mobile communication. As 5G deployment is yet in the implementation phase in most countries, the problem arises while implementing hand-off strategies in the aforesaid 5G ultra-dense networks. There exists limited research works on the performance of real-time 5G network behavior as well as hardly a few articles present related to the 5G hand-off strategies. This motivates us to choose this 5G hand-off topic as a primary area of interest.

To construct a high mobility network, the consideration of the spatial Poisson Point Process becomes vital. A dynamic iterative approach through simulation can be made to visualize user mobility and predict the average velocity of users from the total arrival time of PPP.

The main objective of our work will be to choose an optimum network model where the successful hand-off percentage (based on threshold evaluation metric) lies in the good range of SINR. We will keep the same threshold criteria and vary the network model from homogeneous to heterogeneous (HetNet) gradually to observe the increase in successful handoff percentage in the lower SINR range. An increase in the successful hand-off rate at high interference i.e., low SINR ensures network performance improvement.

Finally, the same network models are divided into fractal coverage zones to see the changes in network performance. The result obtained from fractal characteristics can support the cause of degradation of handover performance in fractal networks and demand consideration of path-loss parameters as one of the key hand-off metrics in UDN deployment.

1.3 Literature Survey

We will discuss the previous hand-off-related works in the form of a transition timeline from the advanced 4G to 5G phase i.e., from the traditional 3GPP LTE hand-off (discussed in the first part) to the proposed advanced mm-wave 5G hand-off (discussed in the latter part).

The problems related to the unplanned dense deployment of Base stations in LTE HetNet were discussed in [10]. Though it helps to increase the spatial network capacity to reduce commercial installation costs but affects the robustness of the system during user mobility. In their paper, system-level simulation gives us an insight into key parameters' trade-off performance during hand-off decision-making. In [11], the authors framed a new mathematical model of hand-over as a function of the mobility of the user. Based on Markov Decision Process (MDP) model. Authors derived an optimal context-driven handoff criterion (context parameter such as the size of the cell, power profile, velocity, etc.) to utilize maximum user capacity by limiting unnecessary extra hand-offs. The authors of [12] suggested a similar model that reduces redundant handover overhead in the LTE core network by a co-operation-based cell clustering method. To boost handover management, the authors in [13] proposed a network-controlled handover (NCH) scheme for mobility robustness optimization (MRO) in 3GPP LTE. They suggested a new MRO algorithm that determines channel quality measurement to be the key parameter in finding the best target cell.

Now we talk about a few of the works made on the 5G hand-off [14]-[18]. In [14], the authors simulated a fast handover architecture for 5G small cell networks with traditional metrics like RSSI and SINR. Considering a realistic urban model, their simulation gives comparative better outputs in terms of packet loss, user throughput, and bit error rate than traditional LTE. On the

contrary, authors in [15] proposed that if RSSI-based handover is chosen in 5G, unnecessary handoff can cause heavy signaling overhead and high UE outage probability in the mm-wave link. Several other methods are thus adopted to increase the 5G network performance. One such method applies a new algorithm, called the Value iteration Algorithm (VIA) for solving MDP [16] for obtaining an optimal performance on the quality of the link and dynamic load of the channel. Another modern method was adopted in [15] by invoking a reinforcement learning-based AI technique called SMART to determine hand-off trigger conditions intelligently, maintaining both user QoS requirement and mm-wave channel characteristics. To achieve optimum network performance, our paper resembles [17], where authors work particularly in the area of SINR improvement during modeling a K-tier Het-net. Their contribution shows that to achieve optimum SINR from a given SINR in a network, adding a new tier or BS in that Het-net will not alter outage probability significantly. Their result is accurate to 1-2 dB while calculating the average user rate and average load on each tier.

The propagation environment, discussed till now [10-17] was inherently thought to be of isotropic type i.e., path loss exponent is uniform in the entire network region. The first ever fractal coverage concept was introduced in [18] to measure the performance of 5G UDN. The mathematical modeling of path loss exponent, here, has been derived from the power law behaviour of the spectral density, which has a relatively slow changing variance value in the angular domain. In [19], the authors highlight the effect of such multi-directional path loss in hand-off performance by measuring two parameters, coverage and association probability. The analysis of their simulation shows that the fractal path loss model decreases the coverage performance of a network while increasing the association probability for long link distances.

1.4 Outline of the thesis

- Chapter 2 of the thesis deals with the theoretical concepts of the hand-off mechanism related to a cellular network. It primarily discusses the different phases involved in HO execution with a special reference to 4G LTE and 5G NR Hand-off architecture.

- The reference of spatial Poisson Point Process (PPP), which is used for user mobility framing, is illustrated in chapter 3 with an overview of the process of implementation in a reference simulation environment.

- In chapter 4, the proposed RSSI and SINR-based hand-over process, are discussed with a comparative study of the proposed hand-off algorithm. The system model that should be adapted, is shown with suitable case studies here. It briefly describes the working logic and the behavioral performance of the simulation framework used in the thesis in an isotropic homogeneous environment.

- A further investigation of the fractal coverage network is taken into account in chapter 5. The performance analysis is presented with a detailed study of the successful hand-off rate with different parameters for the same network models considered in the previous chapter. Furthermore, the logical interpretation of the network behavior from the result of SINR coverage probability, average rate, and association probability will be discussed to clarify the effect of multi-directional path loss on fractal networks.

- Chapter 6 gives the overall conclusion that we have derived from the results and includes the future scope of research.

Chapter 2 Study of Hand-Off Mechanisms

2.1 Introduction

This chapter discusses the conventional Hand-off event, used in wireless networks. The definition, requirement, and objective of Hand-Off are discussed in the first part. The chapter proceeds with the discussion of different stages involving Hand-off. Finally, a reference to the working mechanism of the existing 4G LTE Hand-off architecture and the proposed 5G NR HO architecture is made.

2.2 Basic concepts of Hand-off

2.2.1 Definition

In wireless communication, hand-off or hand-over (HO) is defined as a transfer of an active call or a data session while moving from one cellular network to another – more preciously from the coverage area of one network to another. It is necessary because a user session demands uninterrupted service so that there is no loss of connection associated with its movement.

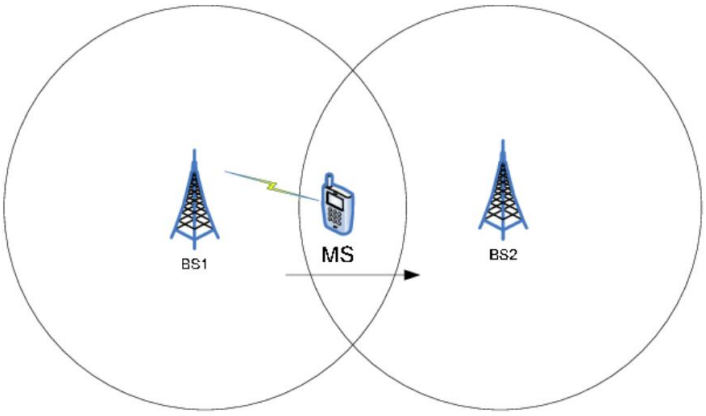

Fig 2.1 Hand-over phenomenon between two cells

2.2.2 Requirement

1. When a user moves from the verge of the coverage boundary of the serving BS and enters into the coverage of a new BS, the Received Signal Strength (RSS) drops below a certain level with respect to the Reference Signal (RS). It results in the weakening of ongoing call or data sessions and may lead to termination. To avoid this, a HO of calls or data sessions is needed.
2. When the network load of a cell exhausts i.e., the maximum number of connections served by BS is reached, the excess active connections are transferred to adjacent cells for triggering HO provided they are receiving adequate signals i.e., residing in the common region between the primary and neighboring cells.
3. Due to the interference between two users (residing in two cells) while using a single channel of the same frequency for communication requires a hand-off for allocating different channels.
4. Generally, for fast-moving subjects, the data link is provided through an umbrella-type cell coverage. When an accelerated object stops suddenly, HO is needed through some intra-micro or macro small cells inside the same umbrella cell to free up channel space for other fast-moving objects.

2.2.3 Objective

The transfer of the ongoing communication channel of a user during hand-off can be in terms of slot association (time division multiplexing), frequency band allocation (frequency division multiplexing), or assigning a code word (code division multiplexing) for a target BS. When there are unallocated channels present in the target BS, it assigns one of them to the mobile user. But in the case when all channels are occupied, it is left with two options, either to terminate the active hand-off call or to pause a new call request made to that BS. This problem

is addressed technically by the two HO metrics, named, forced termination probability (probability of hand-off failure and thereby termination of call or data session) and call blocking probability (blocking a new call request). The motto is to trade-off between these two network parameters during HO in such a way that the forced termination of calls should decrease significantly while not increasing the probability of call blocking [20].

2.2.4 Different Stages of Hand-off

The primary stages of hand-off in any wireless network are measurement, decision, and initiation. Hand-off measurement is a process of continuous sensing of a network environment. Based on the hand-off metrics, a measurement report of different parameters is prepared. A hand-off decision is made from the metric characteristics report, measured from both the source and target. Finally, in the hand-off initiation phase, a request for hand-off triggering is made fulfilling the decision criteria].

Because of random user movement, the RSS at the source and target sides fluctuates inversely i.e., as per the propagation path loss, if a user moves nearer to the target, The target RSS increases while the source RSS decreases. A time averaging window function is used to eliminate the momentary fading of the signal. The techniques of HO initiation can be of four types [21]. Based on the way of measurement of HO metrics, they are-

Relative Signal Strength (RSS) - The relative signal strength in the time domain plays the role of triggering HO. In fig. 1, it is found that when RSS of BS1 decreases below RSS of BS2 (region after point A), a hand-off can be initiated [21]. Although the signal strength of BS1 was sufficient to continue the call or data session, unnecessary hand-offs may take place here due to signal fluctuation in the aforesaid region (known as the ping-pong effect). This increases the call blocking probability and should be avoided.

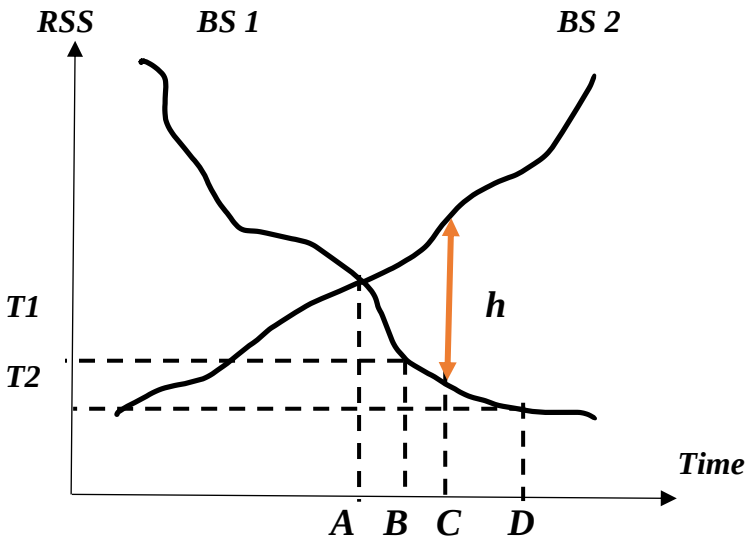

Fig 2.2 RSS characteristics for hand-off initiation [21]

Relative Signal Strength (RSS) with Threshold - To encounter the ping-pong effect, a threshold value is introduced along with RSS for hand-off initiation (T1 in Fig. 1). In this case, hand-off is initiated when RSS of BS2 is above RSS of BS1 and RSS of BS2 is below point B.

Relative Signal Strength with Hysteresis - In this method, a hysterias value h is introduced for hand-off initiation. When the RSS difference between BS1 and BS2 exceeds value h (region after point C), a hand-off initiation request is made.

Relative Signal Strength with Hysteresis and Threshold. - This is the best method for minimizing the number of hand-offs. Here along with hysterias, the threshold value (T1) is also taken to satisfy both of the criteria. When both criteria are met (region after point C).

The threshold at point D is known as the Receiver threshold (T2 in the figure) which is the minimum user RSS for call continuation. The system intelligently utilizes the time interval between the hand-off request and receiver threshold in the hand-off queuing process [22]. It delays the hand-off request and waits until neighboring occupied channels become free. The various protocols used in the handoff-decision stages are-

- ***Network Controlled HO (NCHO)*** – Used in 1st generation mobile network AMPS (Advanced Mobile Phone System) where the network itself takes the responsibility of RSS measurement and hand-off decision.
- ***Mobile Assisted HO (MAHO)* –** Used in GSM (Global System for Mobile Communications) where MS (Mobile Station) works in collaboration with BS or MSC (Mobile Switching Centre) to reduce the load on the network. The HO measurements are done on the MS & HO decision is taken at MSC.
- ***Mobile Controlled HO (MCHO)*** - Used in DECT (Digital European Cordless Telephone) where MS has the full authority to initiate and execute HO alone. The MS finally takes the HO decision based on the measurement information collected from BS and itself,

2.3 Analysis of 4G LTE and 5G NR Hand-off

4G LTE network architecture consists of three main components, the user Equipment (UE), the Evolved UMTS Terrestrial Radio Access Network [23] (E-UTRAN), and the Evolved Packet Core (EPC). The E-UTRAN (access network) consists of UE (User Equipment) and eNBs (BS are re-termed as eNB in LTE). The EPC (Evolved Packet Core) serves as the core network.

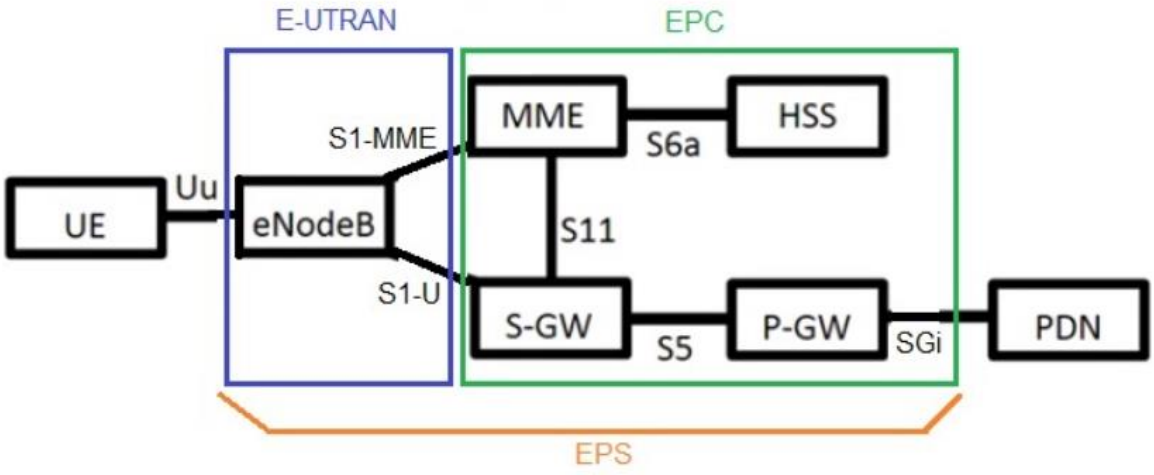

Fig. 2.3 LTE Network Architecture [23]

Inside the EPC (Fig. 2.3), MME (Mobility Management Entity) with the aid of HSS (Home Subscriber Server) control the user mobility by exchanging proper signal through the serving gateway (S-GW) of the EPC.

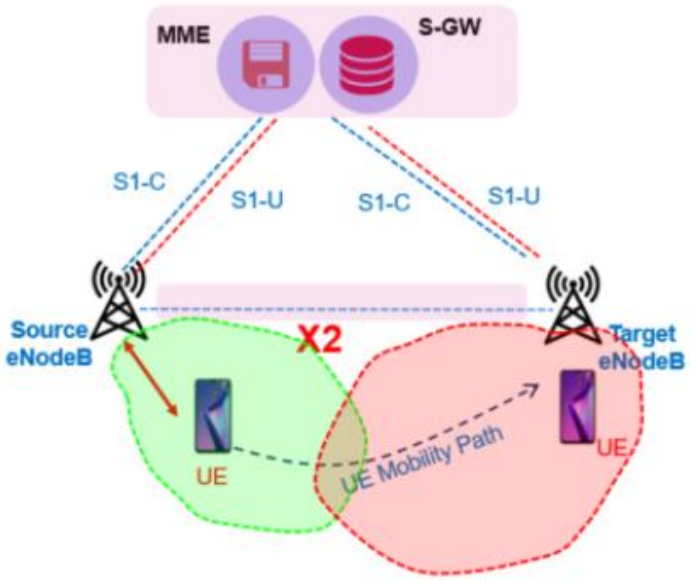

Fig. 2.4 LTE HO Procedure [24]

The 4G LTE HO procedure can be explained in terms of source eNB, target eNB, and MME (Refer to Fig. 2.4). The serving eNB determines whether HO is needed or not based on RRC (Radio Resource Control) Measurement Reports (MRM) that are collected periodically from UEs. The HO decision is made from the RRC characteristics compared to a vertical and horizontal offset value at the source end. If the source and target RSRP difference exceed the vertical offset, (A3 offset), for a horizontal offset duration, (TTT - Time to Trigger), it accounts for a HO initiation [24]. Whenever such HO is initiated, the type of the HO – whether X2 HO (Intra eNB HO) or S1 HO (IP Based HO) is determined also by the source eNB. The serving eNB forwards the HO request to the target e-NB. The target eNB synchronizes itself by creating an uplink S1 bearer link to the same S-GW used between the source eNB and MME. Upon receiving the HO ACK signal (acknowledgment) from the target eNB, the serving eNB sends an immediate HO command to the UE for hand-off execution. The UE accesses the

desired channel through a process of RACH (Random Access Channel Transmission). The UE finally sends a HO confirm message to target eNB as well as S-GW after HO completion. The S-GW releases the old S1 bearer and establishes a downlink S1 bearer with the target eNB for creating a new data path for communication.

Implementation of 5G Hand-off is extremely challenging as it has to withstand high throughput and user density by means of massive numbers of network access nodes for accessing varieties of applications. During user mobility, the discussed 4G LTE HO procedure will become inefficient as per the 5G specification (3GPP and ITU specify any end-to-end service should not cross 1 ms latency). In order to prevent delay, signaling overhead during initiation and rejection phases should be minimized for providing 'ALWAYS ON' connectivity to a user (Access points should not be missed in HO transition).

The 5G service-based core architecture described in [TS 23.501, Sec. 4.2], comprises different Network Functions (NF), like AMF (Access and Mobility Management Function), SMF (Session Management Function), and UPF (User Plain Function).

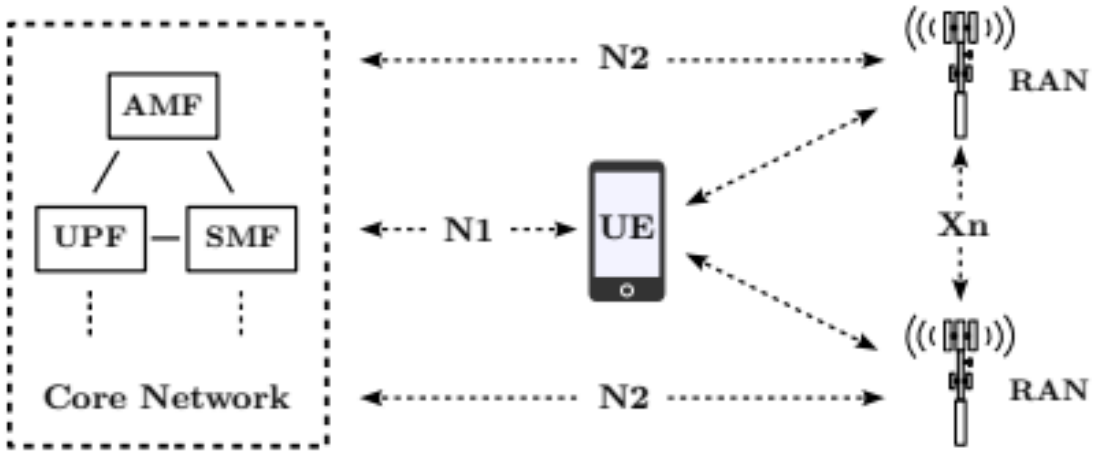

Fig. 2.5 5G architecture and network interface [25]

During movement, the NFs do not communicate directly with outside core entities like UEs and different RANs (Radio Access Networks supported by 5G like GSM, UMTS, LTE, etc.) instead, they connect with the 5GC (5G Core Network) via secure interfaces (N1 and N2) provided by AMF [25]. Fig. 2.4 illustrates the network interface architecture cantered around a UE.

The transfer of UE between different RANs needs proper handling of HO based on available interfaces. As per the 5G 3GPP specification (3GPP TS 38.300 section 9), the 5G NR HO can be classified into two categories- Xn-based 5G intra gNB HO (5G BS are termed as gNB) and N2-based 5G intra RAN HO, also known as C plane (Control plane) handling. In Xn-based handover, messages can be directly communicated between two gNB nodes without involving the CN to reduce signalling overhead. On the other hand, in intra-RAN HO, the RANs communicate indirectly through 5GC via the N2 interface.

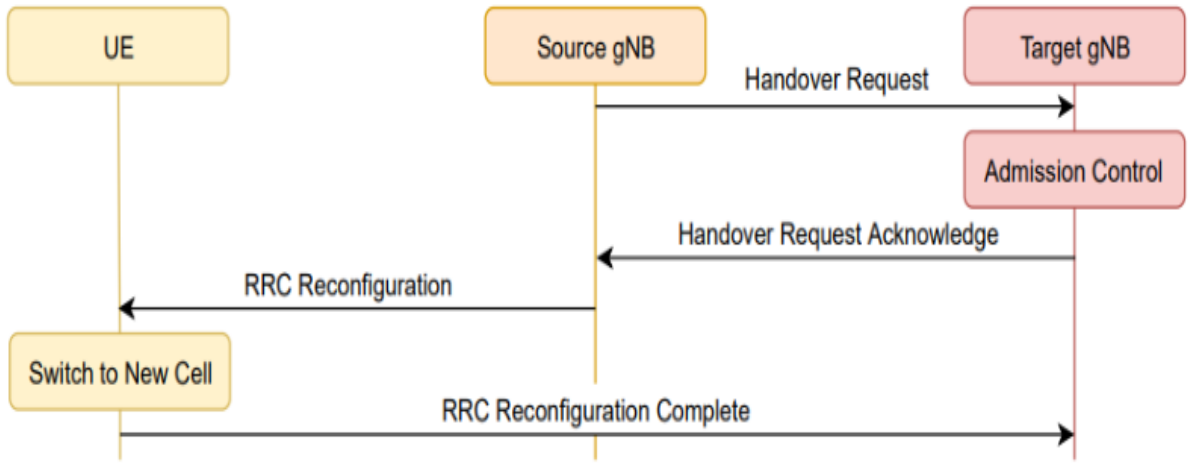

Fig. 2.6 Xn-based 5G Intra gNB Hand-over [25]

Xn-based HO can be treated as Network-controlled HO and can be further classified into cell level HO and beam level HO as per the RRC signaling attachment (Radio Resource Control). In Fig. 2.4, it may be observed that in an

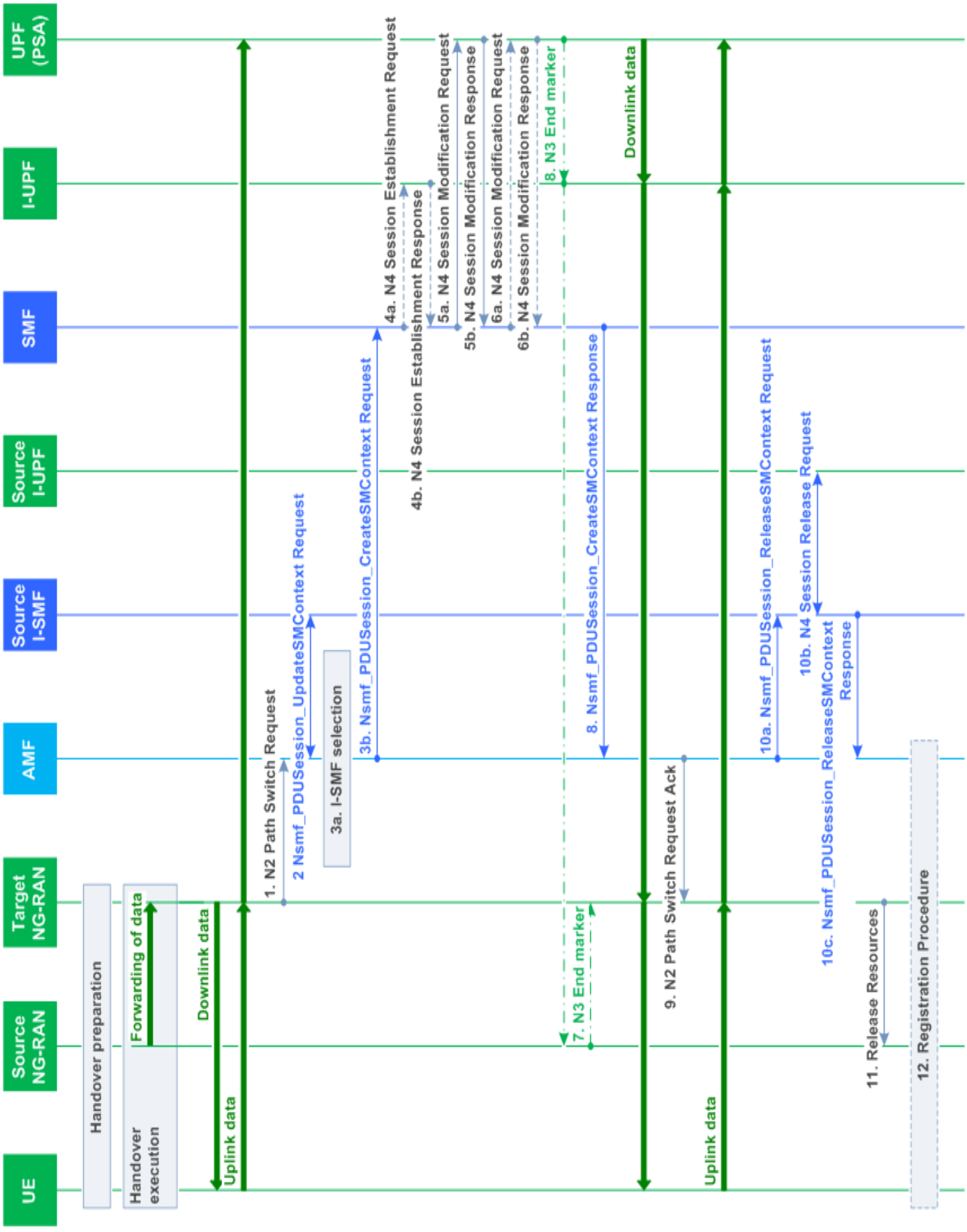

Fig. 2.7 N2-based Intra RAN Hand-over [25] (C plane Handling)

intra gNB network, an XnAP HO request message is forwarded from the source gNB containing target cell Id, list of PDU (Protocol Data Unit) sessions, etc through the Xn interface. As a part of HO acknowledgment, the target gNB provides admission control and an explicit RRC connection (RRC signaling config. is required in the case of cell level HO). The source gNB passes the RRC config. to the UE in the form of an HO command so that it can obtain the cell ID of the target gNB without knowing any core system information. It may contain antenna beam information also in the case of beam level HO. Finally, UE passes the RRC to the target gNB and reports the HO completion reply against the HO command. No explicit RRC signaling is needed in a beam level intra gNB HO.

Fig. 2.6 illustrates the N2 based 5G intra-RAN HO process in the Control plane of a 5G network. It is similar to the 4G LTE S1 HO. The whole process flow does not depend on the availability of the Xn interface. It takes more time than Xn Ho because of the involvement of 5G Core. Unlike Xn, the 5GC can allow updating AMF and session values [25] in the preparation phase of HO. Different HO messages are exchanged between RAN and UE based on encrypted session keys. The N2-based HO can be used when previously attempted Xn-based HO has failed. Similarly, after HO completion, the CN (Core Network) performs resource releasing from the source RAN to the target RAN. The implementation of 5G HO in the U-plane (User plane) is still in the development phase.

2.3 Chapter Summary

1. The concept of HO arises due to the movement of users between different coverage regions of network cells. The HO should be executed in such a way that it should not increase the forced termination of calls as well as call blocking.

2. The three different stages of HO execution are HO measurement, HO decision, and HO initiation. The HO decision is made based on the RSS or RRC measurement characteristics. HO initiation takes place either at the network end or at the mobile end.

3. From the chronological discussion of the 4G LTE and 5G NR HO architecture, it can be understood that in a high bandwidth efficient network, different signaling overheads exchanged during HO should be minimized in order to reduce network latency. The goal is to provide always-on connected links (maintaining proper QoS) to all the users present in an ultra-dense network region. This can be achieved by designing an optimized, fast, less complex HO algorithm that becomes the future direction of HO work. Our thesis carries this idea and suggests different directions for improving the successful HO percentage, discussed in the next chapters.

Chapter 3 Mobility Model Using Poisson Point Process (PPP)

3.1 Introduction

In this chapter, the Poisson Point Process is discussed primarily with its mathematical origin. The pictorial overview of random points with the variation of intensity parameter (λ) and number of arrivals (N) can be observed as different case studies. The idea of the formation of user mobility with the aid of iterative PPP is formulated in the last part of this chapter.

3.2 Point Process

3.2.1 Definition

A point process is a statistical model for the mathematical computation of a detected pattern of scattered points, where the discrete set of points represents any of the physical world entities that are under the subject of study. Examples can be the location of trees in a forest, vehicles stuck in a traffic jam, the position of bird nests [26], etc. It plays a major role in stochastic geometry [27] as a building block for characterizing complex random set models.

3.2.2 Point Process in Different Dimensions

A point process in 1-D can be useful for sequencing random objects that occur in one dimension. Suppose, if time is taken as a 1-D dimension, the ‘points’ refer to time instants when a specific event takes place. For example, the point process can be thought of as a company’s customer care section, receiving calls from its customers on a 24*7 basis. Such calls happen at random instants of times

all over the day duration (modeled as 1-D points),

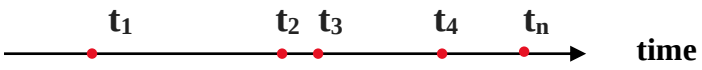

Fig. 3.1 Example of 1-D point process (arrival times)

In d-dimensional state spaces (d is greater than equal to 2), a point process can be used for modeling random spatial points, located in 2-D plain or 3-D space. In 2-D (d=2), the x and y co-ordinate axis, together serve the functionalities of point dimensions. An example can be thought of the locations of customers from where they are calling the helpline of customer care. The locations of the customers are random and modeled as a 2D point process.

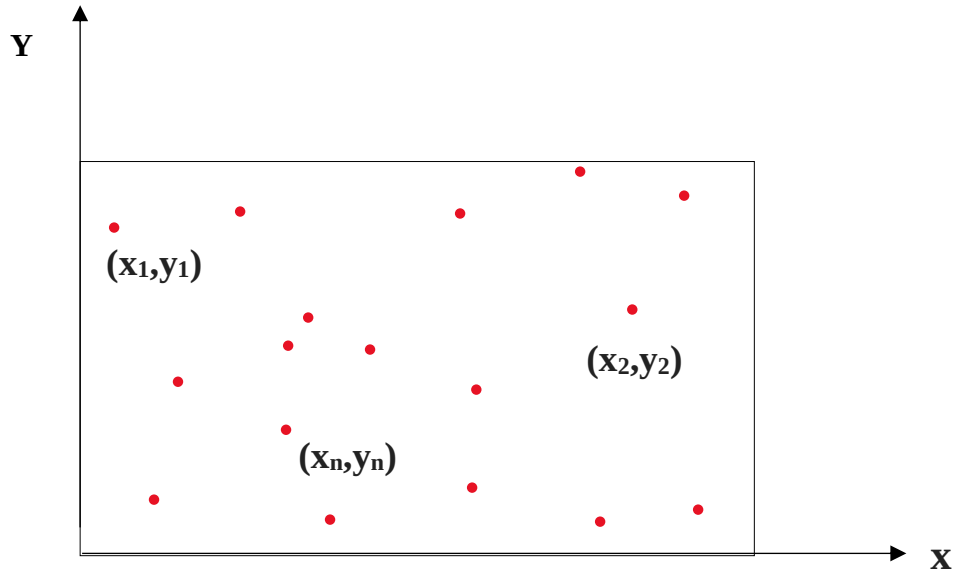

Fig. 3.2 A point process in 2 dimensions (x_i,y_i)

A 3D point process can be thought of as a union of both location and time in the previous example i.e., the location and the time instant of the phone calls made to the customer care company. Here space-time set(time*space) serves the 3-dimensional random space.

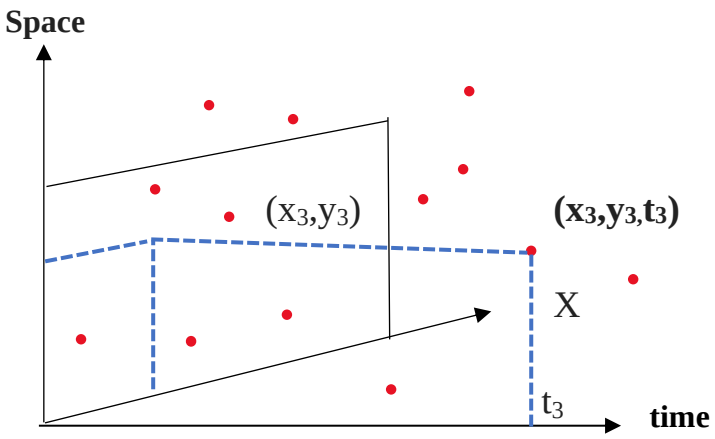

Fig. 3.3 A point process in 3 dimensions(x_i,y_i,t_i)

3.2.3 Point Process Formulation

The difference between 1D and higher order point processes is that the 1D point process possesses a natural sequencing of dimensional values, that is absent for higher order processes. The 1D point processes can be estimated as a random variable but the problem is the values are highly co-related and mutually dependent [28]. An example, in Fig. 2.1, the time instant values have an ordering relation such as $\mathbf{t_1 < t_2 < t_3 i<\ldots\ldots<t_n}$ i.e., $\mathbf{t_i < t_{i+1}}$.

Instead of taking direct instantaneous values, if the inter-arrival time $S_i = t_{i+1} - t_i$ is taken as point variables, the generated random variables in such way S_1, S_2, …. S_n become mutually independent.

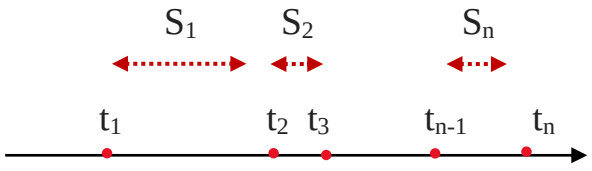

Fig. 3.4 Inter Arrival time S_i [28]

Another way of formulating Point processes as an independent event is done by converting the point process to a counting process [28]. It can be expressed

N_t = **Statement**: No. of points arrived in time t

$$= \sum_{T=1}^{\infty} 1 \quad ; \quad \{T_k \leq t\} \quad ; \quad \in t \geq 0 \qquad (3.1)$$

The summation function $\mathbf{N_t}$ becomes 1 if the statement is true, otherwise 0. The counting process It can convert the point process into a random function in a continuous time domain (t).

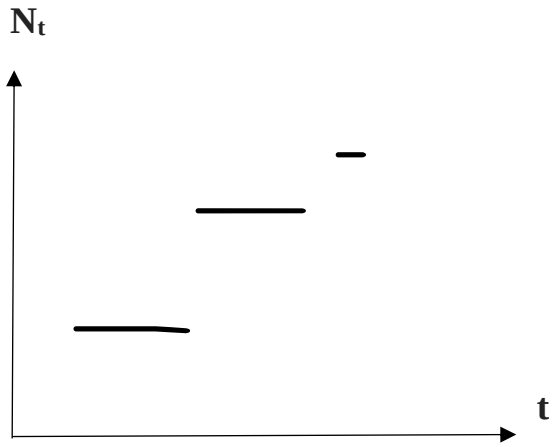

Fig. 3.5 Counting function N_t linked with a point process [28]

A Statement of the counting process can be formulated by counting the no. of points in the defined time duration interval, say $N_{[x,y]}$ for $0 \leq x \leq y$, where, $N_{[x,y]} = N_y - N_x$. Such disjoint interval sets are independent stochastically.

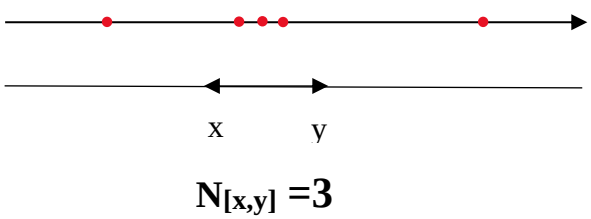

Fig. 3.6. Interval function N(x, y] of a point process

In spatial point processes, as there is no ordering sequence of dimensional objects, the counting process shifts to a region count instead of a finite interval count, expressed as,

N (R) = **Statement**: Number of points that comes under the set R

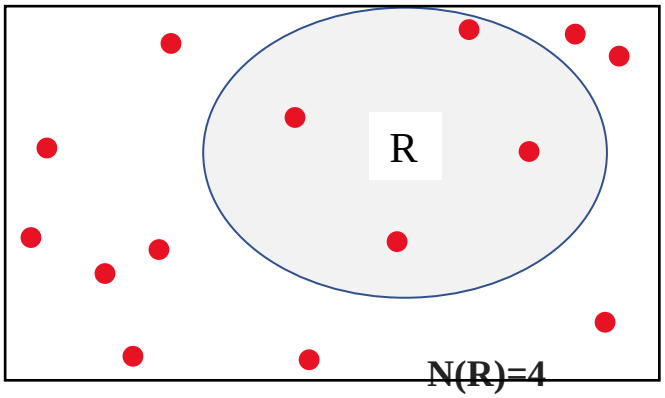

Fig. 3.7. Counting function N(R) of a point process, spatially varied.

3.3 Poisson Process

The association of the Poisson distribution with a point process is called the Poisson process [29] or more precisely Poisson Point Process (PPP). Suppose, the following assumptions are made –

1. The expectation of the number of points arriving in a counting interval is proportional to the length of the interval. The proportional constant (k) is termed as the rate or intensity of the process.

$$N_{[x,y]} = k(y-x) \quad ; k > 0 \tag{3.2}$$

2. Points arriving in two disjoint sets of counting intervals are mutually independent such that the random variables $N_{[x1,y1]}$ and $N_{[x2,y2]}$ can become independent also.

Based on these assumptions, it can be interpreted that the points arriving in a given counting interval should follow a Poisson random distribution.

$$N_{[x,y]} \sim \text{Poisson}[k(y-x)]$$

Where Poisson(μ) denotes the Poisson distribution having mean λ, defined as the probability distribution of a random variable N such that the probability that N equals n is given by:

$$\mathbf{P\{N = n\}} = \frac{\boldsymbol{\lambda^n}}{\boldsymbol{\lambda!}} \mathbf{e^{-\lambda}} \qquad n=0,1,2\ldots\ldots \qquad (3.3)$$

λ (lambda) determines the shape of the distribution which is itself the expected value of N.

3.3.1 Simulation of Static User Points

The arrival or movement of mobile users, to be specific User Equipment (UE), inside a circular area (2-D cellular network) or a 3-D volume space (multistoried building) is considered a random event and can easily be supported by the Poisson point Process (PPP) [28]. The density of users can be varied directly by the Poisson arrival parameter λ. Fig. 2.7 – 2.10 represent different case studies of the static user arrivals (blue dots), on 2D and 3D coverage plain along with the BS (red triangles), placed uniformly with its coverage (shaded region) inside the entire region.

3.3.2 Simulation of Dynamic User Points

To incorporate the concept of mobility, we have iteratively deployed a PPP (with fixed λ) after a consecutive fixed interval of times [30] (defined as the Poisson inter-arrival time $\mathbf{T_{gap}}$) up to a certain number of times (defined as the number of Poisson arrivals **N**) in the same 2-D plain or 3-D space. The total simulation time of the user journey can be found by multiplying the Poisson inter-arrival time ($\mathbf{T_{gap}}$) and the number of Poisson arrival (**N**). The instantaneous location of a particular user can be extracted from the entire user arrival set using the user index at each Poisson arrival. The locus of such Poisson arrival locations of a particular user index i.e., dynamic movement is shown in Figures, 2.11-2.14.

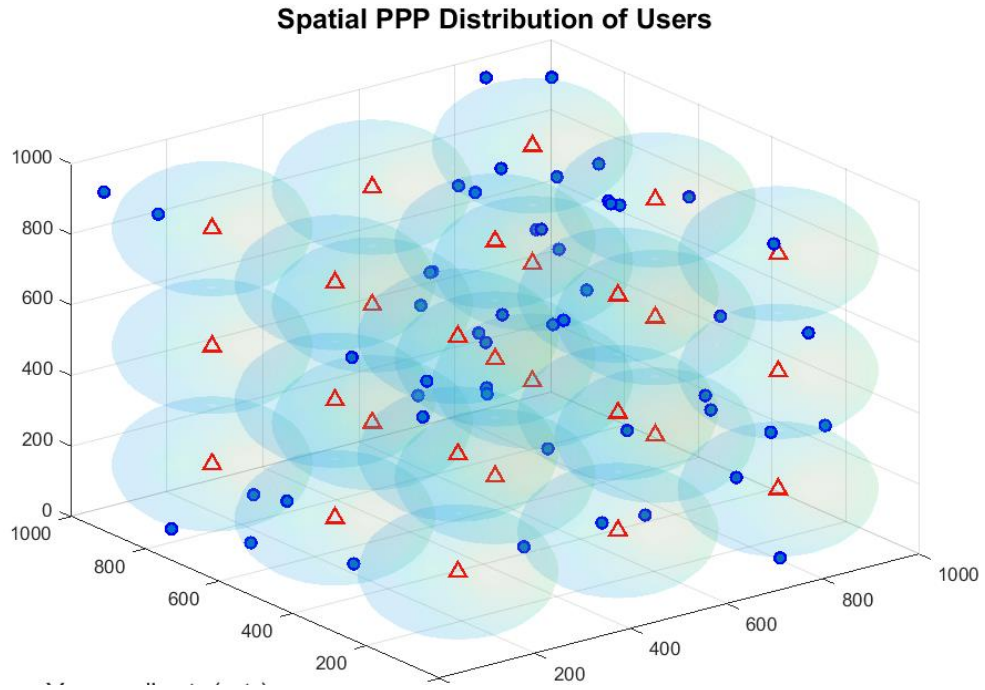

Fig. 3.8. Spatial PPP Distribution of users in 3-D plain for λ=5 and No. of user =50

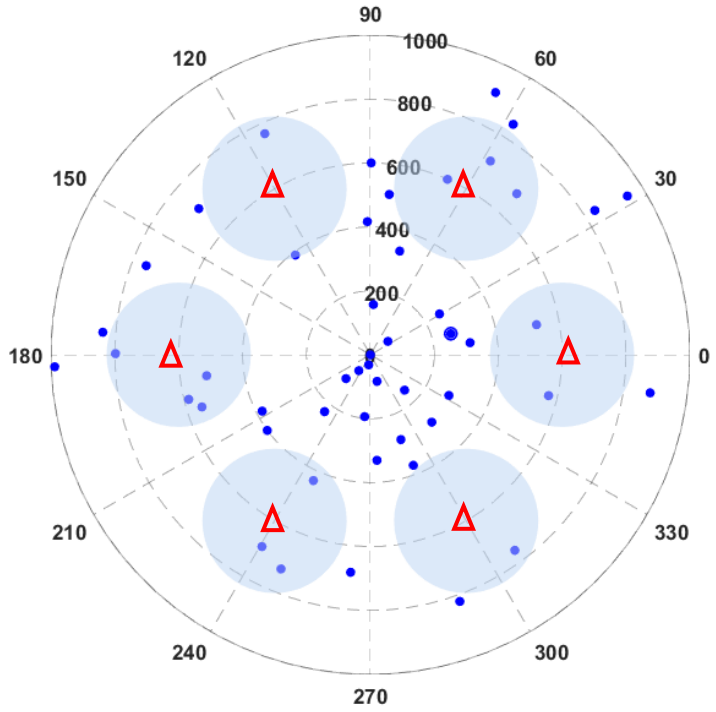

Fig. 3.9 Spatial PPP Distribution of users in 2-D plain for λ=5 and No. of user =50

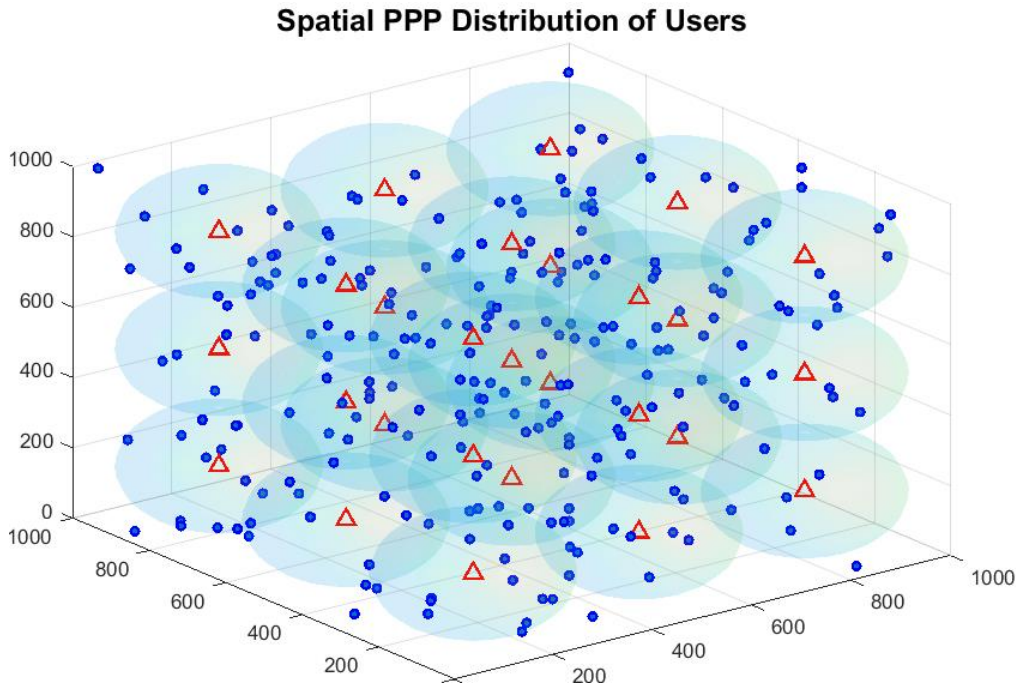

Fig. 3.10. Spatial PPP Distribution of users in 3-D plain for λ=10 and No. of user =250

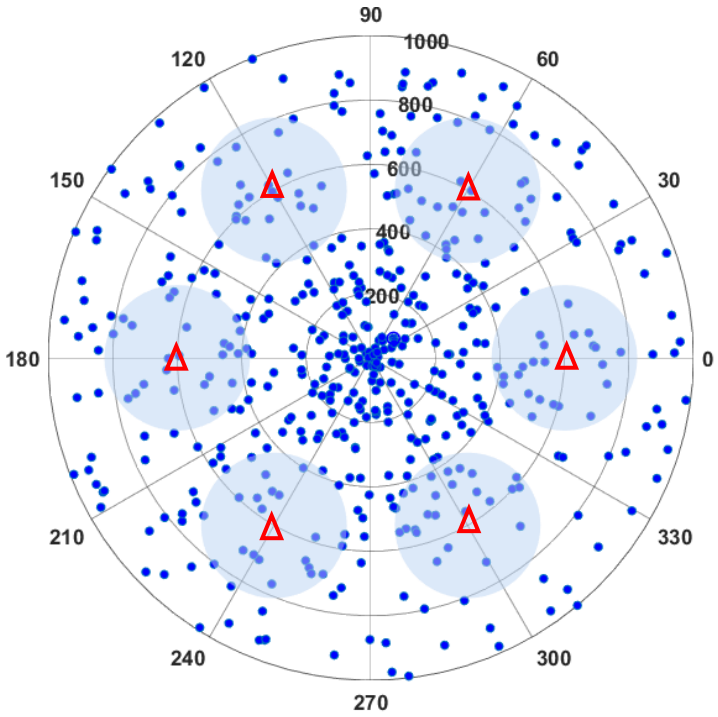

Fig. 3.11 Spatial PPP Distribution of users in 2-D plain for λ=10 and No. of user =250

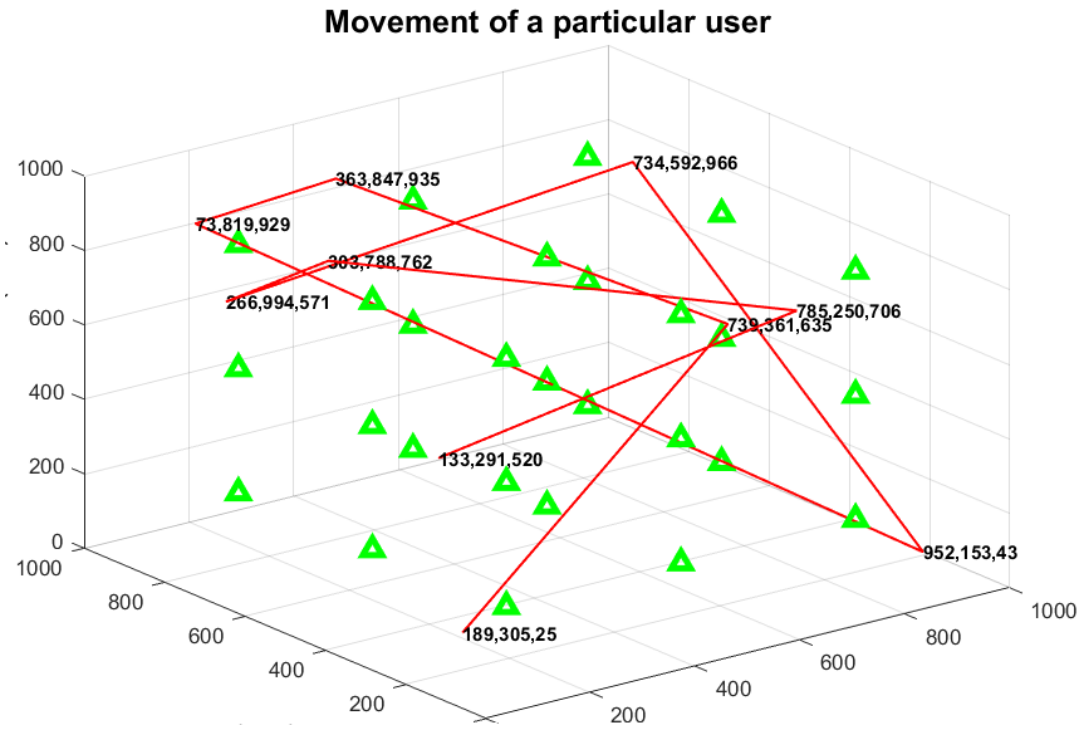

Fig. 3.12 Movement of a user in 3-D plain for No. of arrival =10 (λ=5)

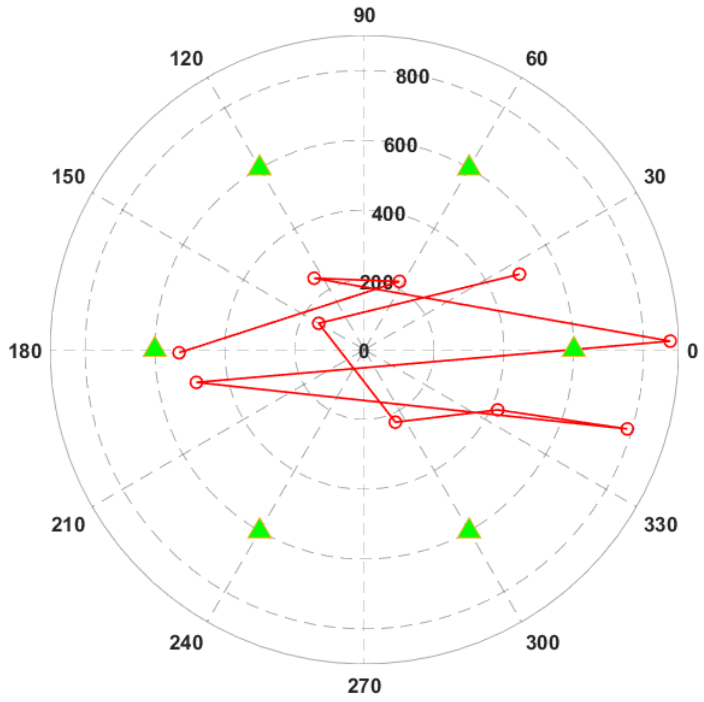

Fig. 3.13 Movement of a user in 2-D plain for No. of arrival =10 (λ=5)

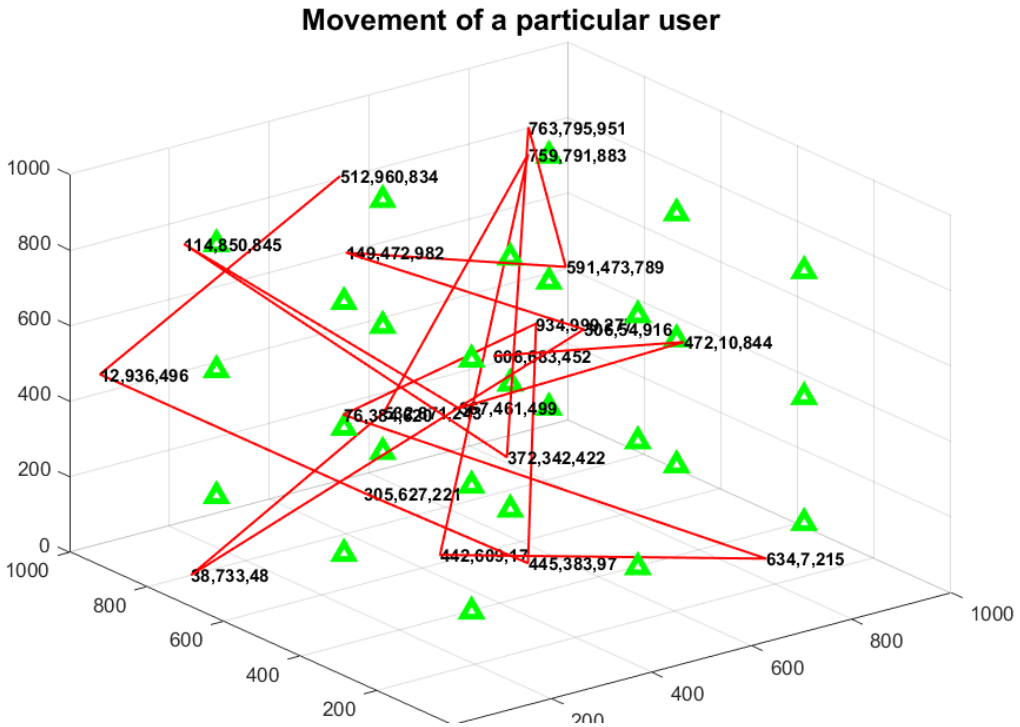

Fig. 3.14 Movement of a user in 3-D plain for No. of arrival =20 (λ=5)

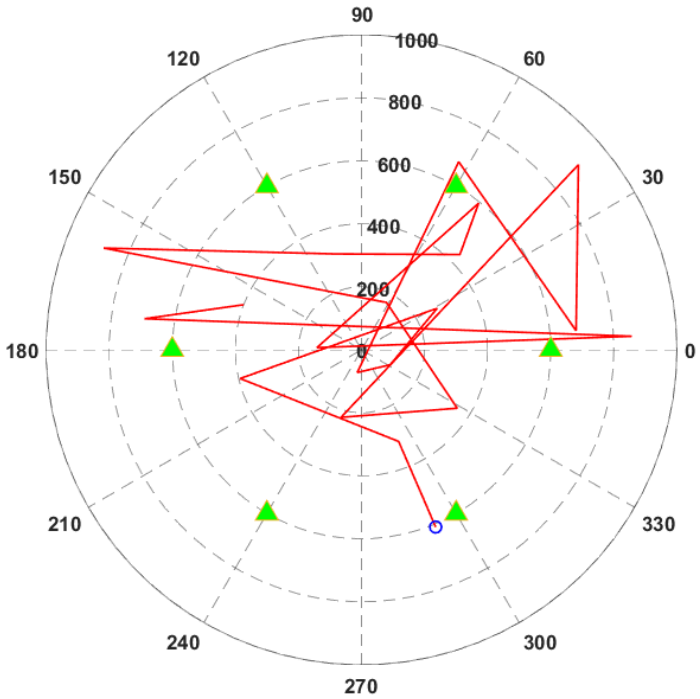

Fig. 3.15 Movement of a user in 2-D plain for No. of arrival =20 (λ=5)

Utilizing the dynamic simulation of the Poisson process, the average velocity of users can be obtained using the algorithm described in table 2.1. To investigate the nature of human clustering or walking patterns, user velocity estimation is highly required in the user mobility model which will be discussed in the results part.

Table 3.1. Algorithm for finding average user velocity

Initialization

Initialize constant variable ***N*** *(No. of Poisson arrival);*

Initialize constant variable ***U*** *(No. of user points);*

Initialize constant variable ***T*** *(Time interval between two Poisson arrivals);*

Initialize ***Poisson_location_array****;*

Initialize ***distance_array****;*

Initialize ***velocity_array****;*

for i=1 *to* ***U*** *do*

for j=2 *to* ***N*** *do*

distance_array (j)*=calculate* ***length[location(j)-location(j-1)***];

end for

velocity_array(i)*= calculate (****sum****[****distance_array****]/(****N*T****));*

end for

avg_velocity*=calculate* ***mean[velocity_array]*** *;*

return ***avg_velocity;***

End

3.4 Mobility Models

In conventional communication, four types of mobility models are widely used, random walk, random waypoint (RWP), fluid flow, and Gauss-Markov. The random walk model was described in sub molecular state of particles inside atoms [31] where the direction of mobility and velocity are independent. The wireless network follows the random waypoint model [32] where pause time is introduced while the arrival of users takes place through the random walk model. The fluid flow model estimates the probability of association duration of UE and BS together [33]. Gauss Markov Model is a memory-based mobility model where the next arrival location is estimated from the present location of the user. Basic human nature tends to stay at some specific positions more than in other locations. Based on the user clustering habit [34], the community concept is developed, which acts as the main backbone of a real user mobility model, called the Individual Mobility Model (IMM). [35]

3.5 *Results and Discussions*

The characteristic of average velocity with the Poisson inter-arrival time is depicted in Fig 2.13. As the characteristic curve is a function of the Poisson inter-arrival time ($\mathbf{T_{gap}}$), it readily follows the random waypoint mobility (RWP) model by fulfilling the requirement of the pause time. From the graph, it is observed that average user velocity decreases while increasing $\mathbf{T_{gap}}$. This can be accounted for the design purpose of the network based on the user's needs. For example, in a vast area of 5 sqkm), vehicular movement is prioritized (average speed is around 50-60 kph), and the Poisson arrival time gap comes in the order of 1-2 minutes i.e., we can estimate the user arrives at the next destined location after 1-2 minutes. In the same area, if pedestrian movement (7-8 kph) was considered in spite of vehicular movement, the Poisson inter-arrival time would have come in

the order of 9-10 minutes which unnecessarily increases the duration of the simulation. Another way of mobility interpretation can be made based on the Poisson intensity factor (λ). If the inter-arrival time is kept fixed, the mobility in terms of average velocity is affected by the factor λ. Although, in the reference inter-arrival time gap, the distinguishing characteristics are not clearly observed unless zoomed into a particular micro section. For example, between a small time window (between 2.23 to 2.29 minutes in the figure), it is seen that the average velocity of users for λ=15 is lower than that of value when $\lambda = 5$. It is because high λ increases the network load, effectively the entropy of the network that makes the average velocity more stochastic.

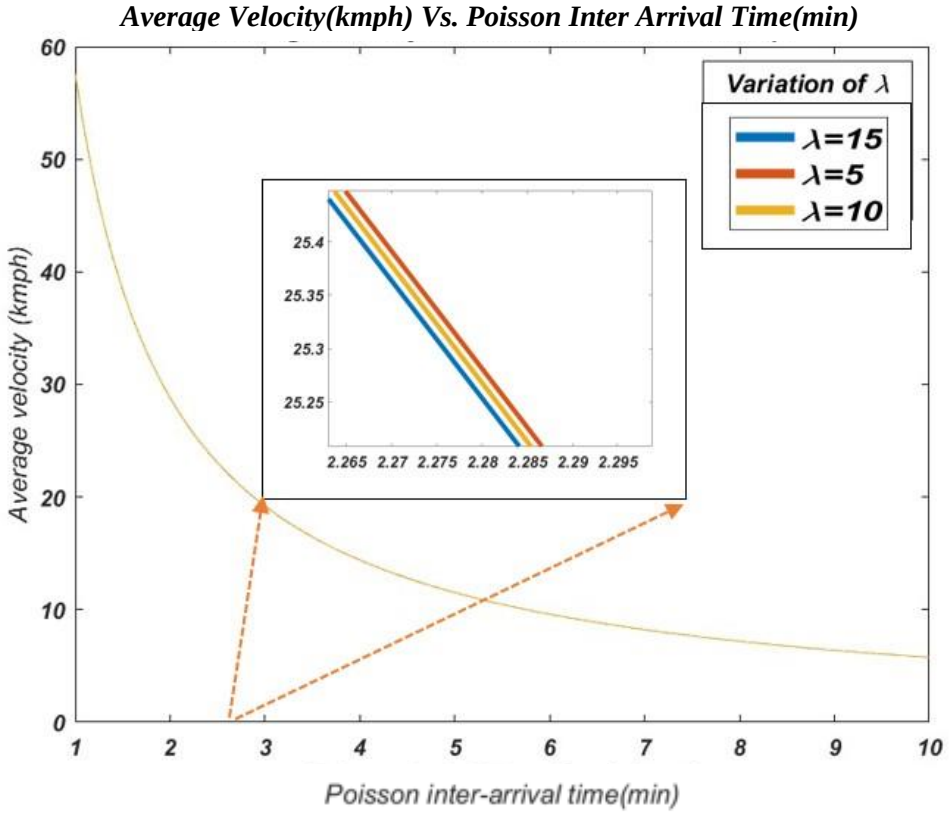

Fig. 3.16 Average velocity Vs. Poisson Inter Arrival Time (T_{gap}) for different values of λ where dimension of simulation area=5000*5000*5000 mtr^3

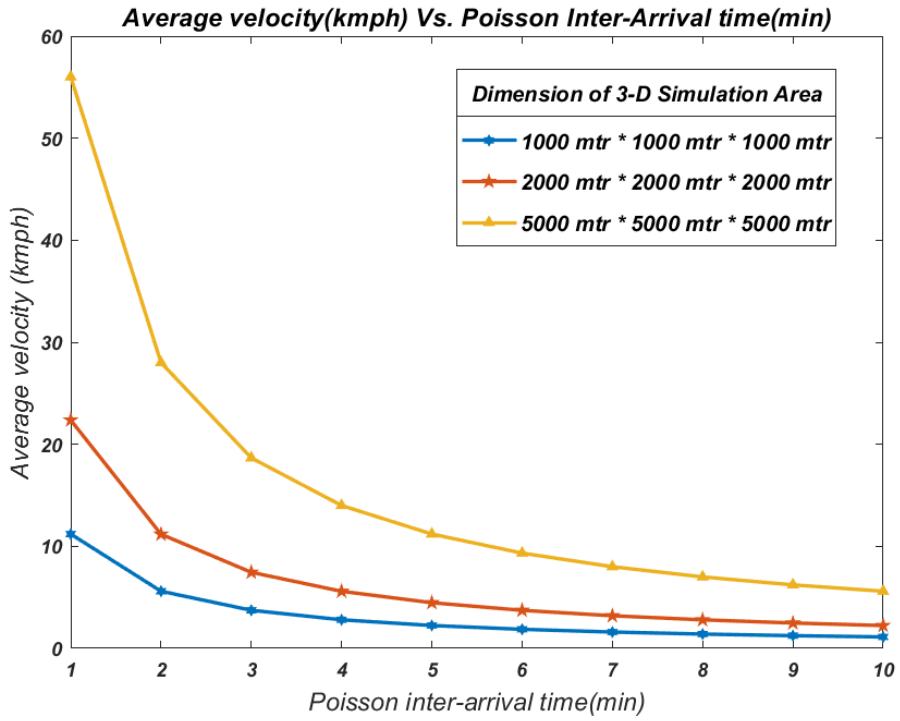

Fig. 3.17 Average velocity Vs. Poisson Inter Arrival Time (T_{gap}) for different values of network dimensions for a fixed λ (λ =10)

Fig. 2.14 illustrates the functional dependence of user mobility on the network dimensions in addition to the Poisson inter-arrival time. Observations show that for a fixed Poisson inter-arrival time (Take 1 minute as an example), a high mobility network (Avg. velocity value is near about 60 kmph) is downgraded to a low mobility network (Avg. velocity value, is about 10 kmph), when the dimension of the side of cubical volume space is lowered to 2 km from 5 km. Alternatively, the reverse implication can be formulated for estimating the dimension of the entire network coverage space for a given average velocity of users. This is an impactful prospect of PPP, where the user mobility model can be directly incorporated with the network performance.

3.6 Chapter Summary

1. Random user arrivals inside a network are considered a Point process and their co-relation in space follows spatial Poisson distribution.
2. At any instant of time, the spatial density of users inside a region is varied by the PPP intensity parameter λ.
3. Mobility of a user is implemented by a recursive PPP algorithm having fixed λ throughout the simulation. The user trajectory is constructed with the aid of two parameters, Poisson inter-arrival time (T_{gap}) and the number of Poisson arrival (N).
4. The average velocity of users can be calculated from the total distances traveled by them in the entire simulated time frame.
5. The characteristics of average velocity with Poisson inter-arrival time support different mobility models according to different requirements.
6. For a fixed dimension of a network, the average velocity of users is inversely related to the Poisson inter-arrival time i.e., in order to achieve high mobility, the inter-arrival time needs to be lowered and for low mobility, the inter-arrival time should be high.
7. Observations also show that the average velocity decreases for a lower dimensional area keeping Poisson inter-arrival time fixed. This can be used to estimate the change in user velocities when the dimensions of the network get changed.

Chapter 4 Performance Analysis of Hand-off in a Homogeneous Environment Using PPP

4.1 Introduction

In this chapter, the simulation of hand-off is carried out in a homogeneous environment having a uniform path-loss exponent. In the first part, the system and path-loss model are discussed. Next, the chapter continues with the process of simulation over MATLAB as per the proposed hand-off algorithm. Finally, the system performance is measured, analyzed, and discussed briefly.

4.2 Isotropic System Model

4.2.1. Network Scenario

We segregate 3 different Network scenarios throughout the work for a comparative study of hand-off performance The first scenario (Type 1) comprises the dense structure of traditional Femto Base Stations (Tr-FBS). Here, the interference signal for an arbitrary user is measured (Fig. 4.1) as a summation signal received from all the other BSs present in the network, apart from the user's serving BS.

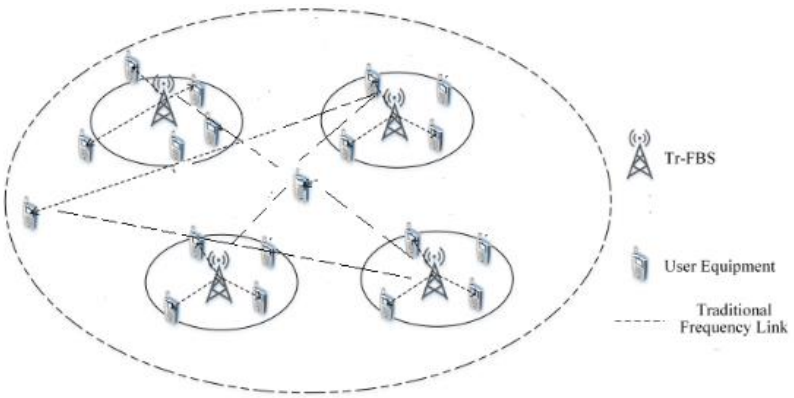

Fig 4.1. System model for Type-1(Traditional FBS only)

The 2nd network scenario (Type 2) is almost similar to Type 1 but with a difference in the mode of adapting the interference. For a particular UE, it is measured as a summation of signals coming from a set of BSs falling inside a filtered cluster region, centered around serving BSs (Fig 4.2). The need for maintaining a cluster is to lower the interference beyond its cluster radius to a minimum value. We will discuss its advantage while showing the hand-off improvement with QoS parameter SINR.

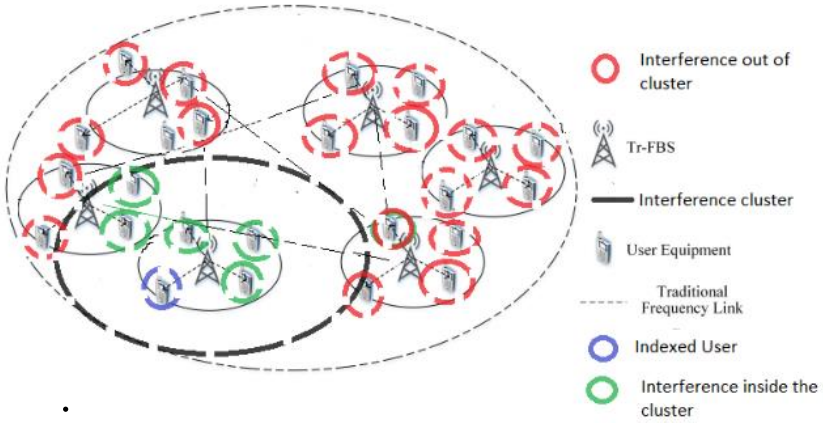

Fig 4.2. System model for Type-2(Traditional FBS with additional cluster)

The third network (Type 3) is the heterogeneous network (tier 2 HetNet) of Femto BS (FBS) and Macro BS (MBS) (Fig. 4.3). The deployment of such a network will show a drastic increase in the successful handoff rate in the same range of SINR, taken in previous cases.

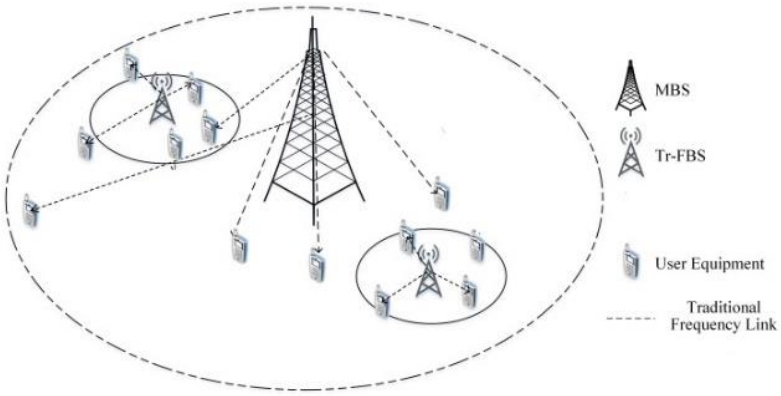

Fig. 4.3 System model for Type 3[HetNet of Macro and Tr-Femto combination (Tier-2)]

4.2.2. Propagation Model

Let us discuss the isotropic channel path loss model in the cases (Type 1 and 2) where traditional FBS in the sub-6 GHz band has been deployed. In these two cases, we take a reference of the alpha-beta-gamma (ABG) large-scale propagation path loss model [36] of the 5G network for urban scenarios. UE and Tr-FBS can communicate in either 2 forms, Line-of-Sight (LOS) state, and Non-Line-of-Sight (NLOS) state. LOS implies that a link directly exists between UE and Tr-FBS without any obstruction. Many environmental factors like large terrains, buildings, trees, etc. hamper the direct link in the case of NLOS. In NLOS, channel transition probability, related to the fluctuation of the environment, is typically unknown. We, therefore, limit our preference to LOS in the simple simulation test bench for analysis of Hand-off.

The ABG model pathloss equation [37] is given by –

$$PL_{\alpha\beta\gamma}(f, r)_{[dB]} = 10\,\alpha\,\log_{10}(r/1m) + \beta + 10\,\gamma\,\log_{10}(f/1GHz) + \chi_{\sigma}^{ABG} \qquad (4.1)$$

Here, $PL_{\alpha\beta\gamma}(f, r)_{[dB]}$ stands for the path loss (dB) measured across length and frequency, α and γ are the two coefficients that relate the path loss with length & frequency. The parameter β (In dB), is a variable offset value, that makes the system optimized during path loss. The separation distance between Transmitter-Receiver (Tx-Rx) is given by the parameter r (in meters), the frequency of the carrier is expressed by f in GHz, and the standard deviation over a distance about mean path loss is given by χ_{σ}^{ABG}.

Now for the case where MBS-FBS HetNet has been deployed (Type 3), we have to incorporate 4G LTE path loss models as well in certain cases where a UE connects with an MBS as its serving BS instead of Tr-FBS. To maintain the same environment conditions prevailing like 5G inside the same volume space, we choose the COST 231 Walfisch-Ikegami model [38] to be superior based on

Standard probabilistic 3GPP LOS-NLOS models under Type 3 HetNet. For predicting better path loss in an urban environment, the COST 231 Walfisch-Ikegami model gives better results in comparison to the other path loss models. The path loss equation [39] for COST 231 Walfisch-Ikegami in dB is in urban LOS scenarios:

$$PL_{cost\text{-}231} = 42.6 + 26\log_{10}(r) + 20\log_{10}(fc) \qquad (4.2)$$

Here, the frequency in MHz is denoted by fc, the length between Tx. and Rx. (In km) is given by r.

For traditional links, there is a need of considering co-channel interference in the same volume space. We presume that the MBS and Tr-FBSs are furnished with Omni-directional antenna arrays so that they can send and receive signals from all UE present in the volume during the analysis time of the simulation. Let us take the 'M' number of Tr-FBS and 'N' number of MBS present in the volume. The SINR of i th UE associated with j th BS can be expressed [13] as-

$$SINR_i^j = \frac{Pj\,Gij}{\sum_{k\in M} Pk\,Gik + \sigma^2} \quad ; \quad j \in \text{Tr-FBS} \qquad (4.3)$$

(For type 1 and 2 networks)

$$\frac{Pj\,Gij}{\sum_{k\in\{M\cup N\}/\{j\}} Pk\,Gik + \sigma^2} \quad ; \quad j \in \text{MBS/Tr-FBS} \qquad (4.4)$$

(For type 3 network)

Where Pj is the power transmitted from BS, σ^2 is noise power and Gij is the channel gain between i^{th} UE and j^{th} BS. Gij includes both path loss and shadow effect. There is no extra parameter due to the gain of antennas in the above equation because we have assumed both FBS/MBS & UE, to be equipped with antennas having omnidirectional properties.

Assuming that all the UE has uniform access to bandwidth allocation of BS, according to the Shannon capacity formula, the average throughput density or average rate of 'k' th user attached to 't' th BS can be written as -

$$r_j^k = \begin{cases} \frac{Bf}{Ut} \log_2(1+SINR_k^t) & ; \quad k \in Tr\text{-}FBS \quad \text{(For type 1 and 2 networks)} \quad (4.5) \\ \frac{Bf \cap Bm}{Ut} \log_2(1+SINR_k^t) & ; \quad k \in Tr\text{-}FBS \cap MBS \quad \text{(For type 3 network)} \quad (4.6) \end{cases}$$

Where B_f is the shared bandwidth of Tr-FBS and B_m is the shared bandwidth of MBS. The average UE density per BS is denoted by U_t.

4.2.3. Mobility Access Model

With the proposed deployment of the Ultra-Dense Network (UDN), the underlying structures of localized mobility management (LMM) should have to be kept in mind also. Based on the operation, the functionalities of the Local Access servers (LAS) inside the LTE core network have been partitioned into two primary sections - LSC & LDC in 5G. To maintain proper topology status and backhaul connections, LSC (Local Service Centre) is required whereas, for mobility anchors, LDC (Local Data Centre) behaves as a data forwarding path inside LAS. In this LMM architecture, two schemes - centralized LMM and distributed LMM, have been proposed [40] to minimize hand-off signaling costs. In our mobility model, we adopt distributed controlling scheme because we need mobility events to be handled by the independent MBS/FBS unlike handling by the LSC, in the case of the centralized LMM. Though centralized LMM has the least signaling cost of hand-off compared to distributed LMM, our adopted distributed framework performs better compared to the old 3GPP mobility framework in terms of latency, cost of packet delivery, and signaling, according to the mathematical survey done in [41].

4.3 Proposed Methodology

The proposed handover mechanism can be stated in a flowchart given in Fig 4.4. We now illustrate the whole process flow

- To discover a new BS as well as to establish a connection, the sensing module continuously senses the environment by a cell search procedure [42] in the traditional Band similar to LTE. The MBS and FBS transmit omnidirectional synchronization signals all over space. In our cases, all BSs present in the volume space is discoverable to any UE. Once cell search is completed, it goes for target BS selection.

- From a fresh PPP arrival location of an arbitrary UE, the distances between UE & all active BSs and corresponding RSSIs (signal strengths received at the UE receiver antenna as per distances and path losses) are recorded in two separate matrixes named, distance matrix and power matrix. Projecting the shortest path algorithm [43] on the distance matrix, our system selects the nearest BS as a temporary target BS and segregates signal and total interference value from the power matrix.

Suppose there are ‘M’ numbers of Tr-FBSs present in the space, then interference will be always a sum of the ‘M-1’ number of signals on each Poisson arrival of UE for Type-1 Network. For a Type-2 network, further filtering of the ‘M-1’ number of interferer signals takes place based on a predefined interference cluster. All the interferer signals chop down to a small constant value beyond its target BS’s cluster radius, thereby creating a sum of lower interference than Type-1. For Type-3 HetNet, due to heterogenic deployment, two separate interference layers are formed by two or more receiving antennas present in the featured UE. SINR is calculated in these three cases by the formulas 3 & 4 defined previously.

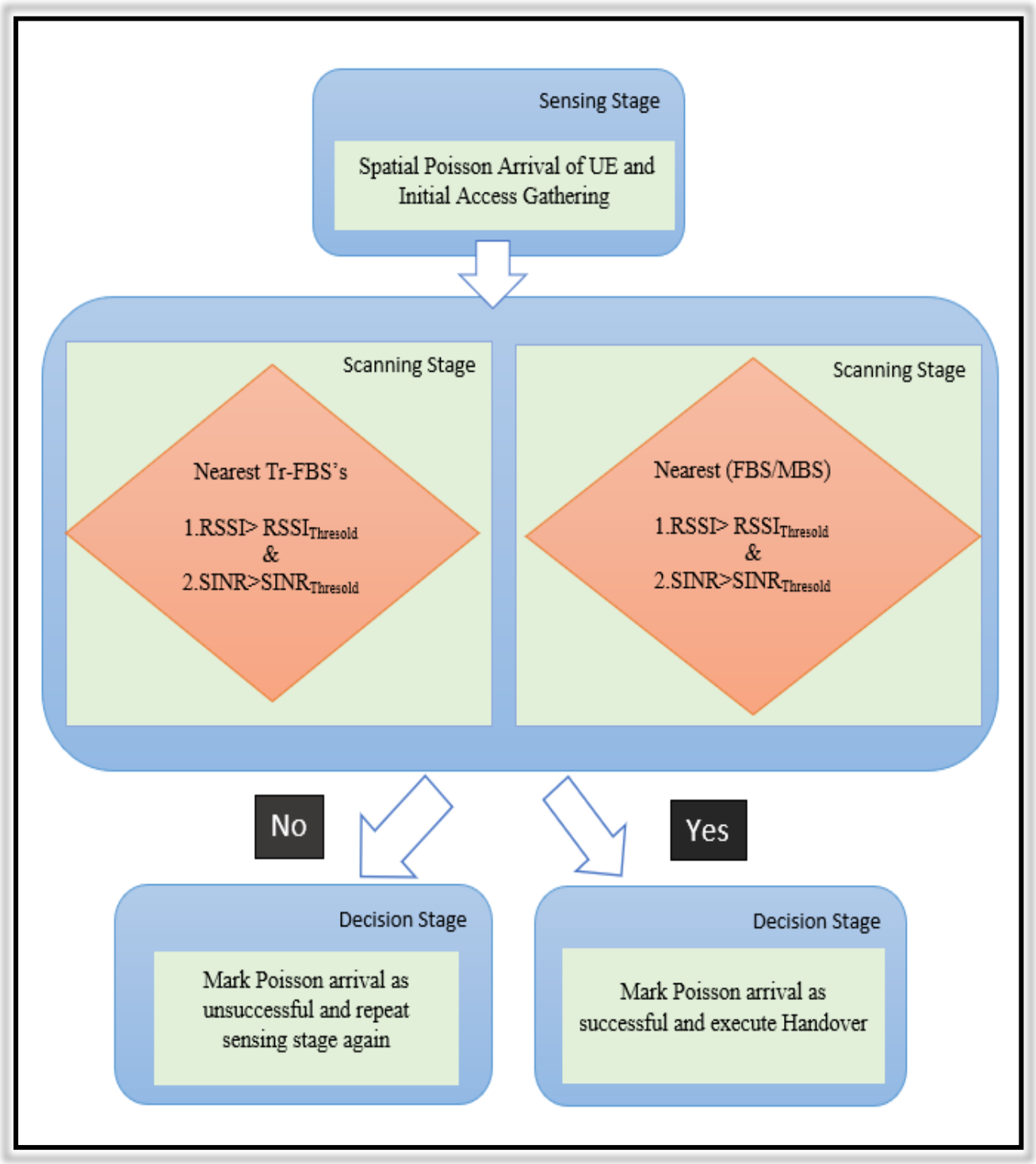

Fig 4.4. Proposed methodology Scheme for Handoff framework

4 In the decision module, RSSI and SINR, jointly work as hand-off metrics to label Poisson's arrival as successful or unsuccessful. The RSSI threshold is calculated automatically based on the cell radius of MBS/Tr-FBS i.e., the signal received at the verge of the boundary of any BS cell. Obtaining the SINR threshold is an adaptive procedure in the best fit range between the minimum and maximum of SINR calculated from the power matrix, in the stipulated simulation.

If the instantaneous value of RSSI and SINR at a UE arrival location is greater than the RSSI and SINR threshold value for FBS (For Type 1 & Type 2), the said Poisson arrival is marked successful, and the temporary status of target BS is moved to final serving BS. For the Type 3 network, the criteria are altered to enhance the successful handoff ratio (number of successful arrivals/total number of Poisson arrival). As there exist two different frequency links for FBS and MBS, it checks the RSSI and SINR thresholding criteria of MBS also along with FBS to assure successful handoff for the cases where UE arrival has been marked unsuccessful by the thresholding criteria of FBS.

4.4 Numerical Analysis

4.4.1 Simulation Framework

In this section, the process of simulation over the MATLAB software platform is shown. In this section, the process of simulation over a testbed software is shown. The entire simulation is performed in MATLAB – a powerful analytical platform that aims to perform complex computations with the aid of a graphical interface. Any real network scenario can be easily analyzed either by MATLAB's simulation testbench or by using MATLAB's primitive library & user-defined functions

The deployment of Base Stations (FBS & MBS) is carried out linearly in the form of spherical cells inside a 3D volume space. The inter-site distances (ISD) between adjacent BSs can be altered to change the cell radius.

A sample simulation snapshot of the Type 1 FBS network is given below in Fig. 4.5. The linearly spaced BSs are placed (red triangles) and highlighted with their coverage regions (multicolor shaded zones). The entire journey of a particular UE inside the 3D space is obtained by (blue line) plotting the instantaneous PPP arrival locations. The arrival positions of a particular user are extracted from the PPP location matrix of all users' using the index of that particular user as a search key. During each Poisson arrival, the nearest BS, if evaluated suitable by the hand-off threshold metric criteria (RSSI and SINR), is marked black immediately & the event is accounted as a successful hand-off. The actual parameters for simulation of all network types (type 1-3) are written down below in Table-4.1

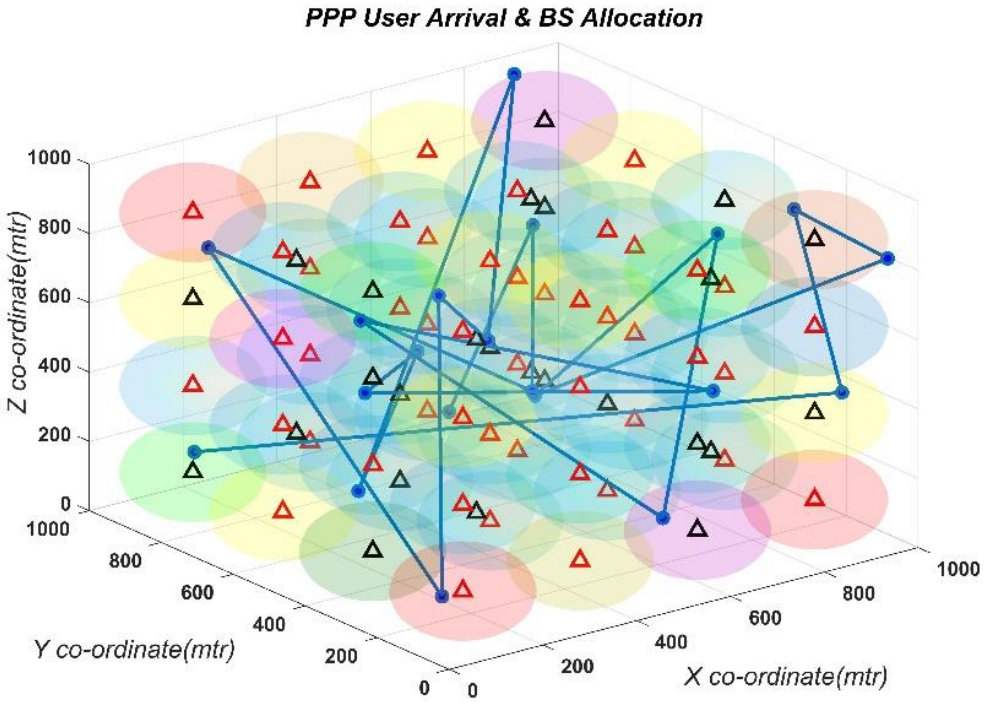

Fig 4.5. Simulation overview of BS allocation of a particular use

TABLE 4.1 *SIMULATION PARAMETERS*

Parameters	***Value***
Entire Network coverage area	*5000m x 5000m x 5000m*
Poisson Inter-Arrival Time	*2 min*
Number of Poisson arrival	*1000*
Lambda (λ)	*10*
Number of FBS on one side	*7*
Number of MBS on one side	*2*
Dimension (radii) of MBS	*1250m*
Dimension (radii) of FBS	*312m*
Inter-Site Distance (ISD) of MBS	*2500m*
Inter-Site Distance (ISD) of FBS	*1250m*
Frequency of carrier	*2.3 GHz*
Tx. Power for MBS	*43dBm(13dB,20W)*
Tx. Power for FBS	*30 dBm (0dB,1W)*
Tx. Bandwidth for MBS	*10 MHz*
Tx. Bandwidth for Tr-FBS	*100 MHz*
Noise Power	*-80dBm*
Path loss Model	*Alpha-Beta-Gamma (ABG) [α=2.8, β=11.4, γ=2.5] & COST-231 Walfisch Ikegami*

4.4.2. Results and Discussions

In the discussion part, we will compare and analyze handover performance in terms of successful Poisson arrival as a function of SINR for QoS improvement. In the first experiment, (the Type-1 network) the comparison result shows the decrease in the successful hand-off rate, on increasing the SINR threshold value (in Fig. 4.6). Increasing the SINR threshold will discard some of the instantaneous UE Poisson arrivals, having less instantaneous SINR values. These arrivals were evaluated as successful hand-offs previously because of the low SINR threshold metric. Also, observations show that the successful hand-off rate decreases with minimizing the femtocell radius which is quite evident because decreasing cell radius will result in an increase in RSSI threshold in the handoff decision metrics. As the ISD is fixed, it lowers the possibility of the arrival of random UEs inside the small coverage regions of BSs & can't be accounted as successful.

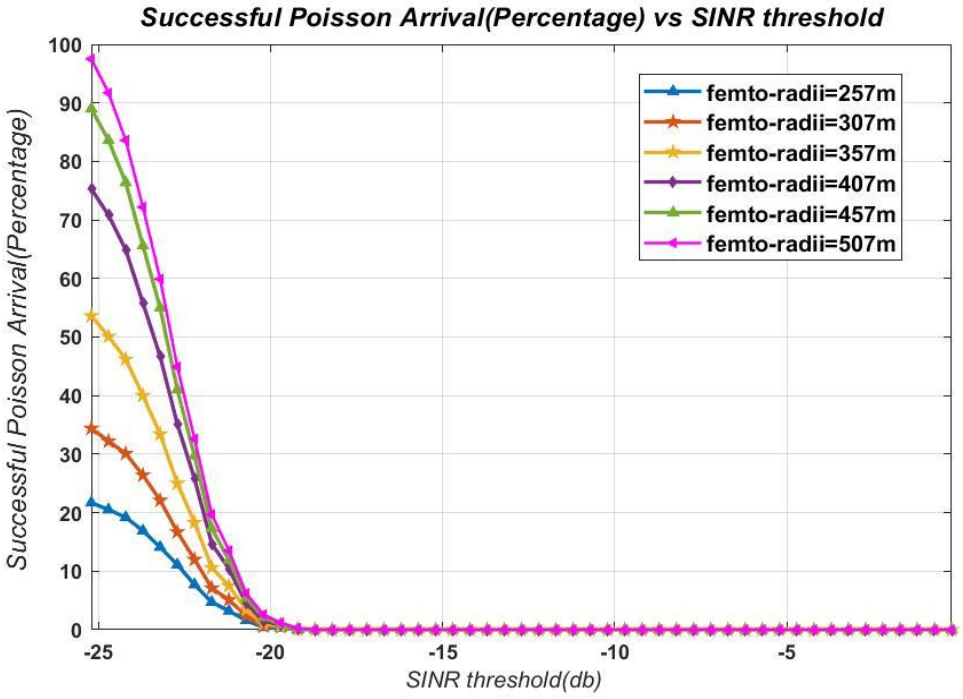

Fig 4.6. Successful Hand-off comparison in Type-1 Network

The problem in the type 1 network is that it encounters poor user QoS. (Region of Successful Hand-off converges below -20dB, which is not desirable). To eradicate poor user QoS problems in the Type-1 network, the concept of clustering is applied in the same FBS network (Type-2). As negative SINR indicates more interference (number of BS is significantly high in UDN resulting in high interference) than signal power, our target will be to minimize interference to a lower extent without altering the number of BS. The cluster thus acts as a filter to attenuate unwanted interference. The cluster radius can be varied in terms of BS cell radius to have control over interference. Lowering the cluster radius will reject more number interfering signals, resulting in the convergence of successful hand-off rate more towards 0 dB. In the 2nd experiment, the obtained figures (Figures 4.7.a, 4.7.b, and 4.7.c) illustrate the phenomenon of shifting of hand-off convergence towards 0 dB, where interference cluster radius is decreased from 5 times to 3 times of femtocell radius.

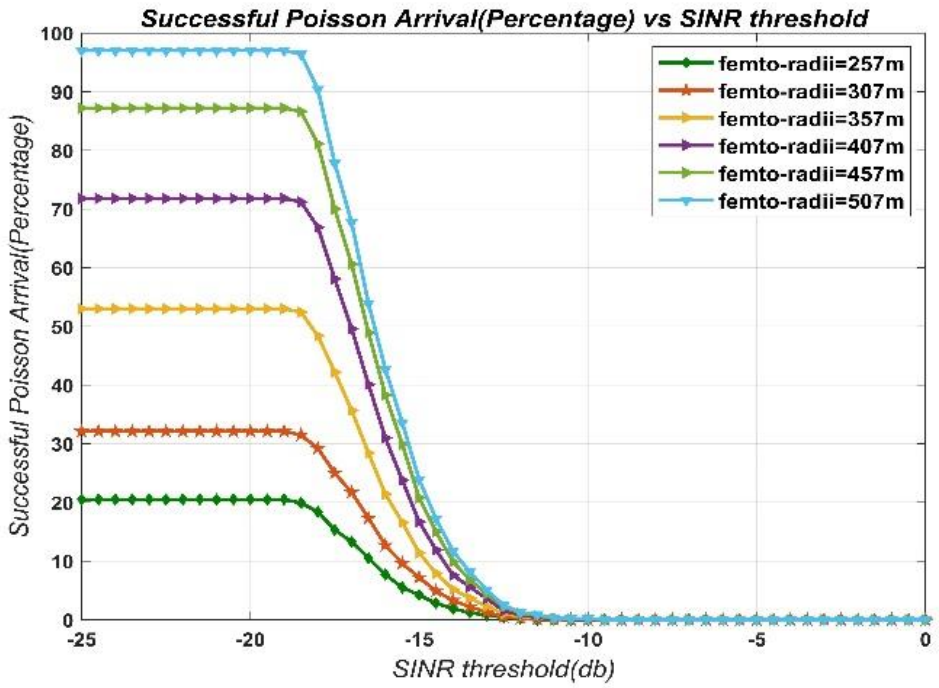

Fig. 4.7.a. Successful Hand-off comparison in Type-2 Network (Interference cluster radius =5* femtocell radius)

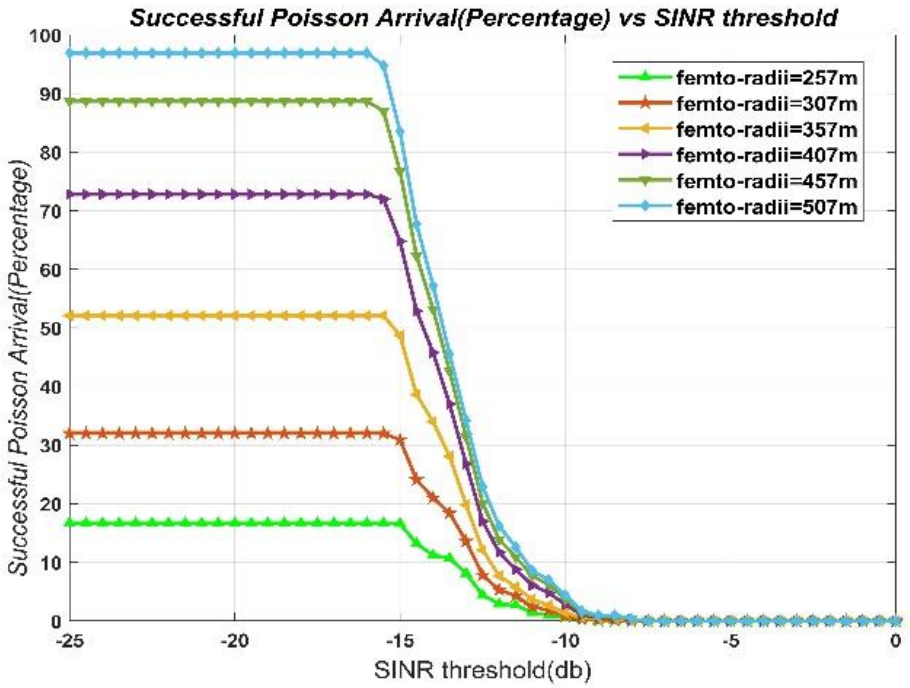

Fig. 4.7.b. Successful Hand-off comparison in Type-2 Network (Interference cluster radius =4* femtocell radius)

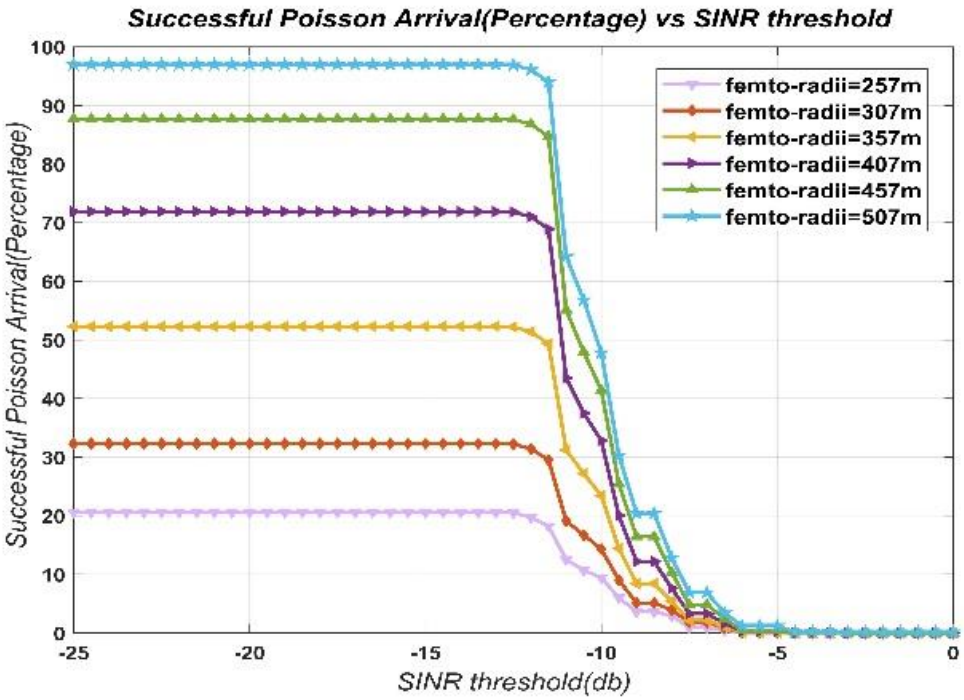

Fig. 4.7.c. Successful Hand-off comparison in Type-2 Network (Interference cluster radius =3* femtocell radius)

In order to get extremely good QoS, convergence needs to be shifted in the positive domain of SINR, which is not possible by applying clusters of the lowest minimum radii. When we shift the network type from homogeneous to heterogeneous (A HetNet of tier-2), it readily serves the requirement. In this case, the UE has the capability of operating in two frequency bands with two antennas such that it can record two instantaneous values of RSSI & SINR. The advantage is the fruitful utilization of a single SINR threshold.

. In the 3rd experiment, Fig. 4.8 shows the result of applying HetNet (solid lines) over traditional Type 1 or 2 networks (dashed lines). It can be readily concluded that the successful handoff rate doesn't converge rapidly in the negative SINR threshold region. Rather, it maintains a static nature both in the positive and negative domain of the SINR threshold.

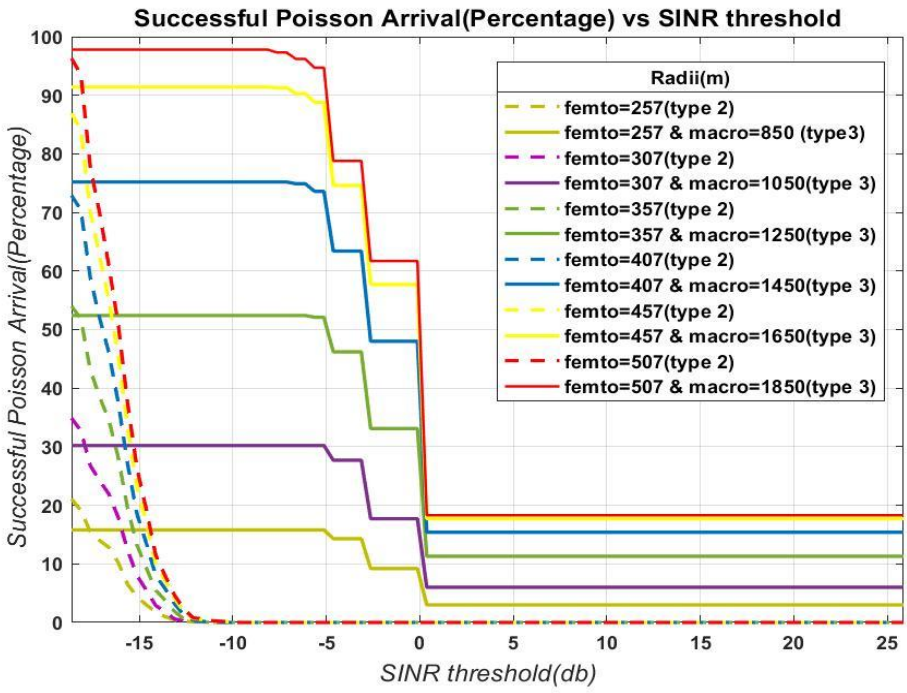

Fig. 4.8. Hand-off comparison in Type-3 Network compared to Type-2

For a fresh UE arrival, even if the threshold metric comparison fails in the 1st tier (in the 5G frequency band), it goes for a 2nd level threshold metric comparison in the 2nd tier (in the traditional LTE band) for the same arrival with same SINR threshold. It ensures the probability of an increase in the successful handoff rate in the positive SINR domain. This is the most stable result obtained so far as slight fluctuations of the SINR threshold will not hamper hand-off performance, giving the best QoS among all the network model types discussed.

We can draw some more interesting conclusions from the characteristics of the average throughput vs SINR threshold. Here the average rate or throughput per BS depends majorly on the user density of the network. A dynamic approach of invoking λ for controlling network load (user density) as well as average throughput, is hereafter adopted as an extra benefit of PPP usage in mobility simulation. The number of BS and the Poisson parameter Lambda (λ), the two parameters, help to determine the average user density per BS (U_t). U_t can be described as the total number of average Poisson arrival points in the state space divided by the total BS number taken in the same volume space. In Equation 4.6, the factor U_t comes in the denominator, and hence increasing it (U_t can be increased by increasing the value of λ or by shrinking the number of BS) results in a reduction of per BS throughput. So, PPP not only controls the framework's mobility, but it has a significant effect on the network performance also.

The incident is characterized in Fig.4.9.a,.4.9.b and.4.9.c where the average user rate has been shown as a function of increasing λ ranging from 5 to 15.. Considering the different network types (Type 1,2, and 3), observations from graphs (Figures.4.9.a,.4.9.b, and 4.9.c) reveal high network speed in terms of throughput in Type-1 and Type-2 networks (Blue dashed lines).

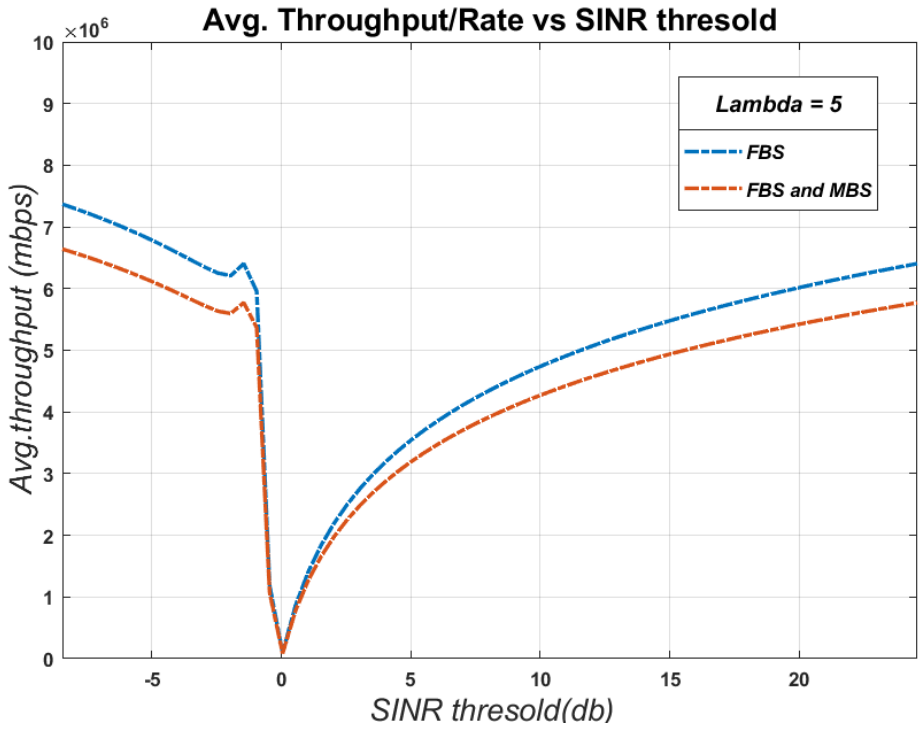

Fig. 4.9.a Average throughput per BS computation taking λ = 5 for different cases of network model (FBS [Type 1 & 2] and FBS-MBS [Type-3])

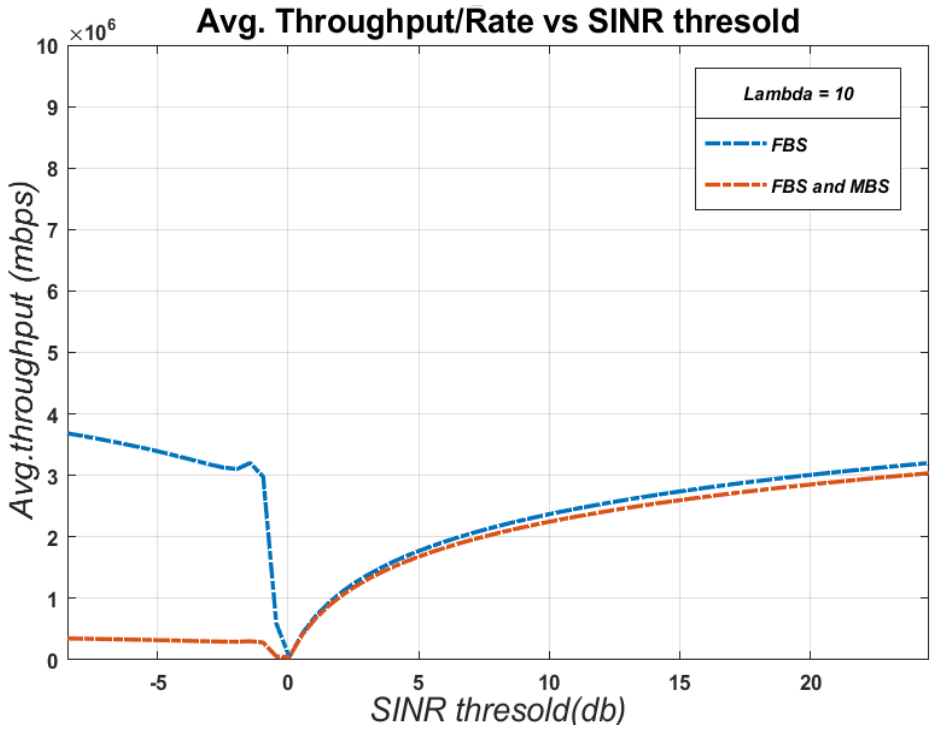

Fig. 4.9.b Average throughput per BS computation taking λ = 10 for different cases of network model (FBS [Type 1 & 2] and FBS-MBS [Type-3])

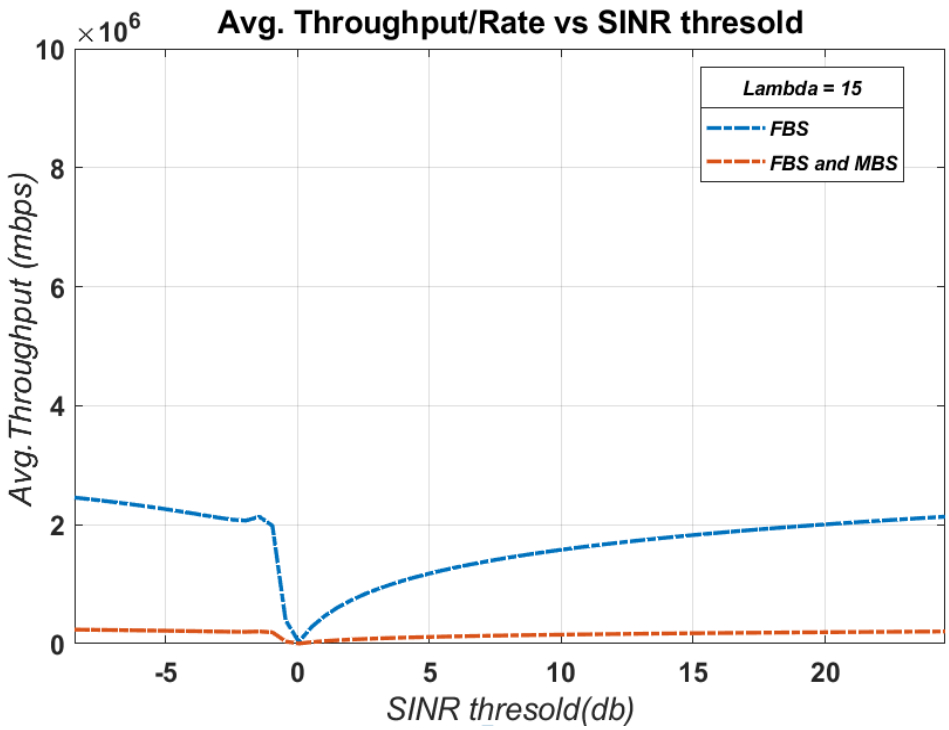

Fig. 4.9.c Average throughput density per BS computation taking λ = 15 for different cases of network model (FBS [Type 1 & 2] and FBS-MBS [Type-3])

The result is quite obvious because of the usage of the high bandwidth value of 5G Tr-FBS (several MHz) in the Shannon equation (Eq. 4.5). In HetNet (Type-3 network), the system compromises its bandwidth in between the two intersecting values of 4G and 5G spectrum. Certainly, in this case, the high bandwidth link of FBS will not persist throughout the session but rather decreases sometimes to a few MHz when MBS is allotted instead of FBS by the hand-off threshold algorithm. It accounts for the degradation of average throughput (Red dashed lines in graphs).

In the domain of the entire SINR threshold, when negative SINR values are encountered, an extra modulus operator is introduced in the Shannon equation (Eq 4.5 & 4.6) to avoid a negative average throughput density. Equations 4.5 & 4.6 can be modified as -

$$r_j^k = \begin{cases} \frac{Bf}{Ut} \log_2 |(1 + SINR_k^t)| & ; \quad k \in Tr\text{-}FBS \quad (4.7) \\ & \text{(For type 1 and 2 networks)} \\ \frac{Bf \cap Bm}{Ut} \log_2 |(1 + SINR_k^t)| & ; \quad k \in Tr\text{-}FBS \cap MBS \quad (4.8) \\ & \text{(For type 3 network)} \end{cases}$$

The inversion or notch in the throughput characteristics around 0 dB can be explained by this introduction of the modulus operator which rectifies or inverts the characteristics in the negative domain of the SINR threshold.

4.5 Chapter Summary

1. In a homogeneous environment, the propagation path loss exponent is uniform throughout the simulation space.
2. The poor QoS problem in the Type-1 homogeneous FBS network is overcome by introducing the clustering concept in the Type 2 network.
3. To achieve the best QoS as well as to obtain stable hand-off performance heterogeneous network (HetNet) of FBS-MBS is deployed in a Type-3 network.
4. For all the cases, the success rate of the hand-off (in percentage) increases with the decrease of the SINR threshold. The hand-off rate is also affected by the parameter cell radius.
5. Keeping the BS Inter-site-distances fixed, decreasing cell radius increases the number of user arrivals in ‘no signal coverage’ zones (void regions) that are discarded by the hand-off threshold algorithm.
6. The average throughput per BS is increased by increasing the SINR limit.
7. In a congested network (high user density), the average rate significantly falls and can be expressed as a function of the PPP intensity parameter λ

Chapter 5 Performance Analysis of Hand-off in a non-Homogeneous Environment Using PPP

5.1 Introduction

In this chapter, the simulation of hand-off is carried out in a non-homogeneous environment comprising multi-directional path-loss exponents. Likewise, in the previous chapter, the system & path-loss model is explored in the first part. In the later phase, the chapter computes the fractal simulation and analyzes its behavioral changes compared to an isotropic network.

5.2 Non-Homogeneous System Model

5.2.1. Fractal Network Scenario

A real scenario of multi-directional path-loss is depicted in Fig. 5.1 where the movement of a user is shown along the straight line from A to D, passing through points B and C. Region between A & B cuts through forests when a link is established between the user & BS. Similarly, the links pass through different buildings between the region of B & C (LOS type) and C & D (NLOS type).

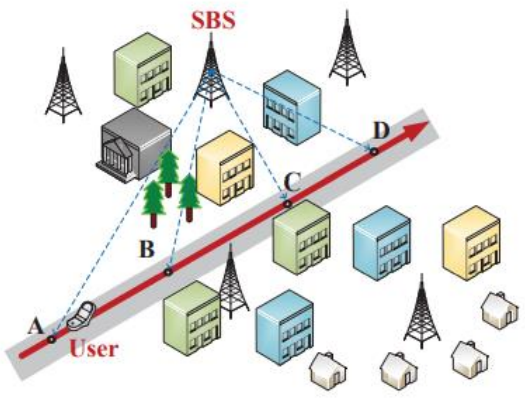

Fig 5.1. A scenario for the anisotropic environment [19]

To build a fractal framework, we adopt a 2D network plane and deploy BS as well as UE by the iterative Poisson processes demonstrated earlier in the previous chapter. Without loss of generality, the 2D coverage plane has been transformed from cartesian to polar for the ease of mathematical computation. Each BS and UE arrival is marked with polar coordinates (r, θ) where r is the radial distance and θ is the angular argument concerning the reference origin of the polar plane.

The entire circular coverage plane is split into 'M' equal regions centered around the origin. Given a propagation environment, 'M' is the modeling parameter for configuring fractal characteristics. The path loss exponents in these 'M' regions are random & statistically different. The entire sequence of path loss exponents can be expressed as a total path loss set $\alpha = \{\gamma_{im}\}$, where index m starts from 0 to M and i is the BS index associated with section m.

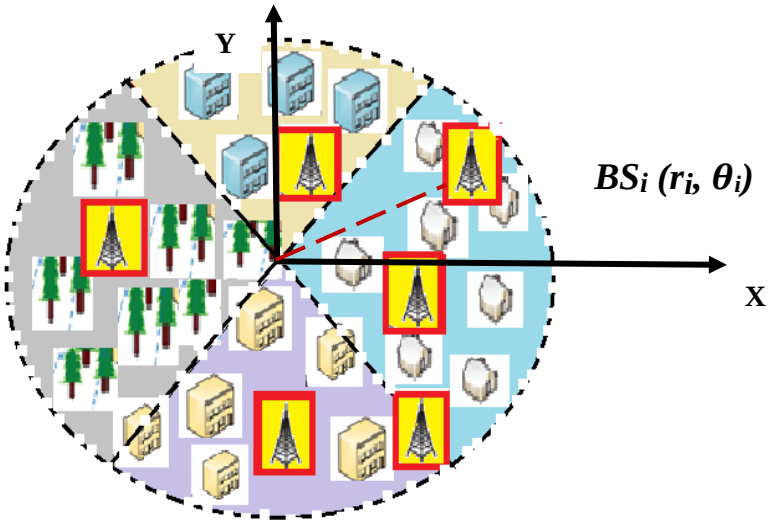

Fig 5.2. System model for the fractal network where M=4

A reference system model is shown in Fig. 5.2 where modeling parameter M is set to 4. It represents 4 different path loss regions (shaded with 4 different colours) containing different blockage elements [44] like trees, buildings, houses, etc., and exhibits independent fractal characteristics. The red boxes represent the set of BSs that are deployed over the fractal plane non-uniformly.

5.2.2. Propagation Environment

Let us discuss in detail the multi-directional propagation scenario in this section. The different fractal path-loss zones in different directions are non-overlapping and stochastically non-identical [45]. Thus, the fractal path-loss exponent set $\alpha = \{\gamma_{im}\}$ can be mathematically modeled as a distribution of discrete identically independent random variables (i.i.d). The distribution has mean μ and variance σ and is uniformly distributed between the range [$\mu-\sqrt{3\sigma}$, $\mu+\sqrt{3\sigma}$] [19]. The PDF of the fractal distribution is written as –

$$f(\gamma_{im}) = \frac{1}{2\sqrt{3\sigma}} \quad ; \ \gamma_{im} \in [\mu-\sqrt{3\sigma}, \mu+\sqrt{3\sigma}] \tag{5.1}$$

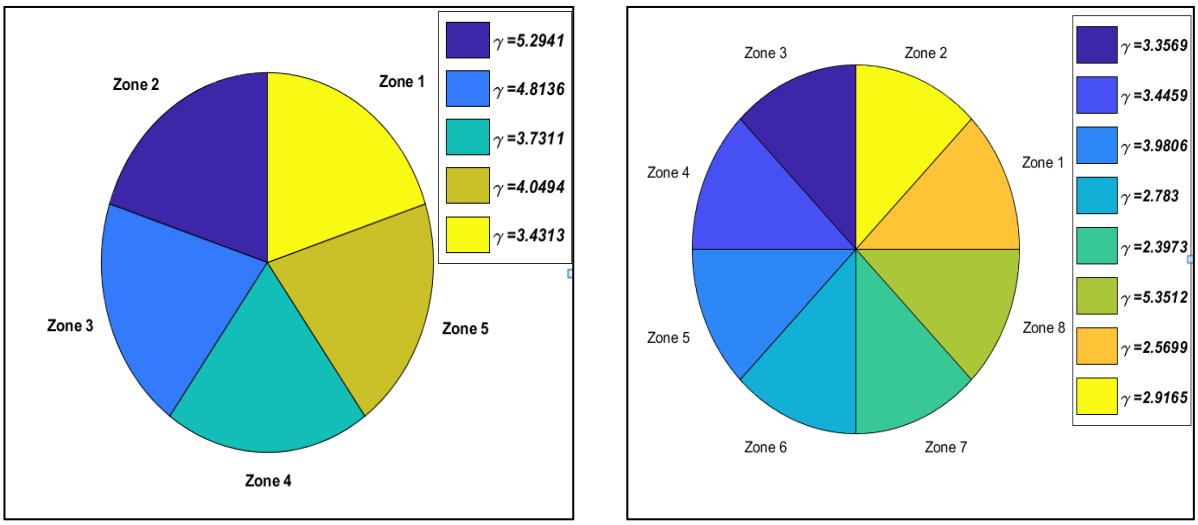

(a) ***(b)***

***Fig 5.3. Path-loss exponents (a) M=5 (b) M=8 for* μ=4 and σ = 1**

- The fractal exponent constant of i th BS of section m is independent of the fractal exponent constant of j th BS of the same section ($j \neq i$) i.e., $\gamma_{im} \neq \gamma_{jm}$.
- The anisotropic fractal model is downgraded to the isotropic model when there is no variance parameter i.e., $\sigma = 0$ during path loss modeling, and elements of path loss set become identical i.e., $\gamma_{1m} = \gamma_{2m} = \gamma_{3m} = \cdots = \mu$

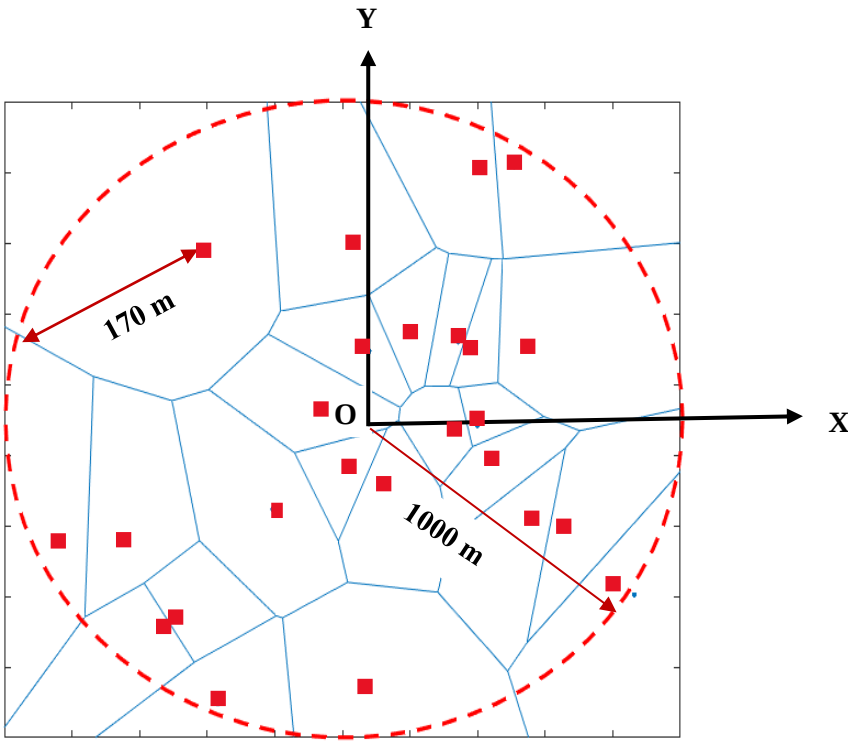

Fig 5.4. Coverage boundaries obtained from the Voronoi diagram

Fig 5.4 illustrates the coverage regions of all the scattered BS present in the entire fractal plane. In a traditional isotropic network, UE selects the target BS by the SINR threshold algorithm i.e., BS with the maximum SINR becomes the target cell for the hand-off triggering. The cell boundary can be obtained by drawing the locus of coordinates having equal SINR between two adjacent BS. The plotting of coverage boundaries for uniformly deployed BS is very simple due to their linear positioning (cell boundaries for uniform BS are mutually orthogonal pairs of parallel straight lines intersecting exactly at the midpoint of ISD between two adjacent BS). But for the cases of non-uniformly deployed BS, the task doesn't seem very easy, rather the method of triangulation is needed to segregate each BS present in the network [46]. One famous plot called the Voronoi diagram, (used here for segmenting BS) uses Delaunay triangulation [47] for the segmentation of points. In the above figure, the red circle represents the entire polar plane. The blue dots and solid lines represent the BS set and its coverage boundaries. The polygon, circumference by the Voronoi boundaries forms the coverage region of a particular BS. The actual coverage boundary of

the fractal network will differ slightly from the boundary position of the isotropic network. It is because of the effect of multi-directional propagation losses which suffers unequal path losses at equal distances. The objective of getting the coverage region is to find the maximum link distance of a particular BS in a particular fractal section of the network.

Practically, networks show fractal characteristics when the distances between UE & BS link are generally lesser than the breakpoint distances. The points on which mutation of fractal exponents occurs are called breakpoints. (Calculated by using parameters like carrier frequency, the height of the user as well as BS, etc.). In the sub 6 GHz or mm-wave band of urban UDN, the breakpoints [48] come in the order of 700-800 meters, typically higher than the average link distances (100-200 meters) of BS. It can be verified from the Voronoi diagram (Fig. 5.4) where the maximum link distance is found 170 meters. Thus, the reference plane of our work does not violate the rule of fractal coverage.

The ABG large-scale propagation model of an urban network is considered in the fractal scenario also (refer to section 4.2.2). A modification of the constant parameter γ is made in the path loss equation (Eq. 4.1) so that it can become a function of the fractal modeling parameter 'M'.

$$(f, r)_{[dB]} = 10\,\alpha \log_{10}(r/1m) + \beta + 10\,\gamma_{im} \log_{10}(f/1GHz) + \chi_{\sigma}^{ABG} \qquad (5.2)$$

Similarly, the SINR equation (Equations 4.3) of the isotropic network works inherently for the fractal model. The same modification is made by introducing fractal exponent γ_{im} instead of γ. The SINR associated with i th user with j th BS is re-written -

$$SINR_i^j = \frac{P_i}{I_i + \sigma^2} = \frac{P_t M_{ti} M_{ri} r_i^{-\gamma_i}}{\sum_{j \neq i} P_t M_{tj} M_{rj} r_j^{-\gamma_j} + \sigma^2} \qquad (5.3)$$

The gain parameter of the sectored antenna (G_{ij}) comprises the product of both the BS & user main lobe gain (M_t & M_r) for obtaining the maximum SINR association in a fractal network. Other parameters carry the same meanings that are described in chapter 4.

5.2.3. Probability of Fractal Coverage and Fractal Association

In this part, the probability of fractal coverage (in terms of SINR & rate) and fractal association have been derived. The performance of fractal coverage can be analyzed with these two parameters [49]. To define these two terms, let us first understand the concept of maximum SINR association [19]. For exhibiting the best performance, maximum SINR association occurs for a user when it chooses a particular BS that is having the maximum SINR among all the BS sets ($\emptyset$) present in the fractal network, and is denoted by BS_k

$$\boldsymbol{k = \underset{i \in \emptyset}{argmax}[SINR(i)]} \qquad (5.4)$$

From the user point of view, considering maximum SINR association, the coverage probability at an instant can be stated as the probability that the desired or required SINR lies above an SINR threshold value Γ.

$$\boldsymbol{P_C(\Gamma) = Prob\ \{\underset{i \in \emptyset}{max}[SINR(i)] > \Gamma\}} \qquad (5.5)$$

The achievable rate (R_o) of a fractal cell considering the multi-directional fractal path loss exponent model can be stated as –

$$\boldsymbol{R_o = B_W\ log_2\ (1+\underset{i \in \emptyset}{max}[SINR(i)])} \qquad (5.6)$$

where B_W is assigned bandwidth to the UE, the coverage probability in terms of rate is defined as the probability by which the achievable throughput of a UE is greater than a threshold rate value γ expressed as-

$$\boldsymbol{P_{Ro}\{R_O > \gamma\} = Prob\{BW\ log_2\ (1 + \underset{i \in \emptyset}{max}[SINR(i)]) > \gamma\}} \qquad (5.7)$$

In an isotropic network, it is quite evident that the nearest BS of a user is having the highest SINR and the probability of successful handover for that particular BS is maximum. However, maximum SINR association can occur for a LOS link of greater path length than an NLOS link of shorter path length [50]. For simple analysis, we can neglect the complexity of the network as of now and define the association probability (P_A) between desired BS_r and user as a function over link distance (r).

$$\boldsymbol{SINR\ (r) = \frac{P_t M_t M_r r^{-\gamma r}}{I\ (r) + \sigma^2}} \qquad (5.8)$$

$$\boldsymbol{P_A(r) = Pr\ \{\ SINR(\ r\ ) = \max_{i \in \emptyset} [SINR(i)]\ \}} \qquad (5.9)$$

5.3 Proposed Methodology

The handover mechanism of the anisotropic fractal network functions similarly to an isotropic network. As our model comprises single-tier BS only, the proposed methodology of the framework (refer to Fig. 4.4) doesn't need two parallel processes (used in HetNet) to run simultaneously. The decision module remains intact with a modification in the operation of the sensing module.

The objective of the real-time sensing module of the anisotropic network doesn't limit itself to locating the arrival of UE only, rather it also computes the path loss exponent associated with that particular arrival location. The CSI (Channel State Information) plays a crucial role in sensing the user location as well as determining the associated fractal exponent. A two-way synchronization signal (containing CSI) is exchanged between UE and BS [51] when UE shifts its location to a new point. The path loss exponent is estimated at the BS end by a least squared method depending on the arrival location received from CSI and comparing it to the system map of aerial fractal characteristics previously stored in a database. As a huge number of users are served by a single BS in an urban

network, individual computation of location & path loss exponent for a single user increases network latency which impacts the performance of the system. Therefore, in the first stage of the sensing module, the locations of all active UE as a whole through CSI are recorded, and then the computation of the path loss exponent from all the collected data sets of user location in that time interval is performed by the BS.

Table 5.1 Algorithm for finding the Fractal Exponent

Initialization

Initialize constant variable ***M*** *(fractal modelling parameter);*
Initialize input variable $\boldsymbol{\theta}$ *(user_arrival_angular_co-ordinate);*
Initialize ***fractal_bounadry_array****;*
Initialize ***path_loss_exponent_array****;*
Initialize ***difference_array****;*

Set starting element of ***fractal_bounadry_array*** *to* ***zero****;*
Set interval of ***fractal_bounadry_array*** *to* $\frac{\boldsymbol{2\pi}}{\boldsymbol{M}}$ *;*

for i *in* ***fractal_bounadry_array*** *do*
difference_array (i)*=calculate* ***abolute[fractal_bounadry_array(i) -*** $\boldsymbol{\theta}$***]****;*
end for

min_index*= calculate* ***index*** *of* ***minimum****[****difference_array****];*
return ***path_loss_exponent_array(min_index)****;*

End

The main challenge arises while implementing the real-time sensing module over the simulation framework for obtaining the fractal path loss exponent (at a particular user arrival position) from the entire fractal path loss set $\alpha = \{\gamma_{im}\}$. We adopt a logical mathematical approach to build an effective algorithm (Table 5.1) which helps in finding the fractal path loss exponent accurately.

The angular separation of each fractal zone is $\frac{2\pi}{M}$ rad where M is the modeling parameter. In the simulation testbench, we declare a fractal boundary array of M elements (Say array A) that stores the intersecting angular coordinates of consecutive fractal regions. Assuming, the starting angular co-ordinate of fractal boundary is 0, the consecutive array elements get incremented by $\frac{2\pi}{M}$ radian automatically. Another array of path-loss exponents of length M (Say, array B) is defined whose elements are generated randomly between the ranges μ-$\sqrt{3\sigma}$ *and* μ+$\sqrt{3\sigma}$. A user-defined function (say function C) has been introduced in the simulation program which takes the angular co-ordinate of user arrival location (θ) as primary input and gives the path-loss exponent associated at that user location as the desired output. It follows the minimum difference index algorithm, illustrated with an example.

Suppose, the value of modeling parameter M is set to 6, the angular separation becomes 360/6 = 60 degrees. Array A now automatically stores the values [0, 60, 120, 180, 240, 300]. Taking μ=4 and σ=1, the array B is generated with the values, say [3.5, 4.1, 3.9, 4.7, 4, 8]. Now assuming a reference scenario where the angular coordinate (θ) at a specific UE arrival location is 145 degrees. The function C computes the differences of the given angle value with each element of array A and finds the index of the element that is nearest to it. In this case, the minimum difference is 25 degrees (145-120=25) which is associated with the 3rd element of array A. The function now returns the 3rd index element

of path-loss exponent array B i.e., 3.9 which is the required fractal exponent associated with the angular coordinate 145 degrees. The significance of implementing a fractal coverage network in the polar plane is that the knowledge of only one co-ordinate location (θ) of the user is sufficient enough to find the associated fractal path-loss which may be difficult to compute if cartesian co-ordinates have been chosen (3 sets of boundary coordinates in x,y, and z direction is required).

To find the fractal path loss in between i th UE and j th BS, the distance or length of the intermediate link ($\boldsymbol{r_{ij}}$) is required which can be expressed as -

$$\boldsymbol{r_{ij} = \sqrt{[r_i^2 + r_j^2 - 2r_i r_j \cos(\theta_i - \theta_j)]}} \quad (5.8)$$

where, (r_i, θ_i) and (r_j, θ_j) are the polar coordinates of i th UE and j th BS respectively. SINR is calculated according to equation 4.3 and based on threshold criteria discussed earlier, the PPP user arrival is marked successful or unsuccessful. The successful hand-off rate is compared between isotropic and anisotropic networks in the result section to show the effect of multi-directional path loss on network performance.

5.4 Numerical Analysis

5.4.1 Simulation Framework

The simulation of the fractal network is carried out in MATLAB using a 2D polar plot. The UE is deployed by iterative PPP to incorporate mobility by the same approach done previously in the isotropic network. The entire simulation is performed by taking the input parameters described in table 5.2

TABLE 5.2 SIMULATION PARAMETERS

Parameters	*Value*
Radius of the entire plane	*1000 m*
Number of the fractal zone (M)	*8*
Number of Poisson arrival (N)	*10*
Lambda (λ)	*5*
Number of BS in the entire plane	*20*
Dimension (radii) of BS	*200 m*
Mean of fractal distribution(μ)	*4*
Variance of fractal distribution (σ)	*1*
Carrier frequency	*24 GHz*
Tx. Power for BS	*30 dBm (0dB,1W)*
Tx. Bandwidth for BS	*500MHz*
Noise Power	*-87 dBm*
Gain of the main lobe BS antenna (Mt)	*10 dB, -20 dBm*
Gain of the main lobe UE antenna (Mr)	*10 dB, -20 dBm*
Path loss Model	*Alpha-Beta-Gamma (ABG) [α=2.8, β=11.4, γ] & COST-231 Walfisch Ikegami*

The pictorial comparison of BS allocation based on the SINR threshold algorithm in the isotropic and anisotropic medium can be shown in Fig. 5.4 & 5.5 in the polar plot. In both the figures, the target output BSs (represented initially by red circles) have been marked with black triangles when the SINR threshold algorithm confirms the new arrival location as successful. It can be concluded that hand-off performance in the fractal network sometimes degrades if we consider SINR-based thresholding. In figure 5.5, it can be observed that SINR-based thresholding fails to allocate serving BS for some of the user arrivals despite residing in the vicinity of BS coverage (Marked with red rectangular

boxes). The rule of maximum SINR association is violated in these failed cases. Further, conclusions will be made on this incident in the results part while analyzing the characteristics curve of association probability.

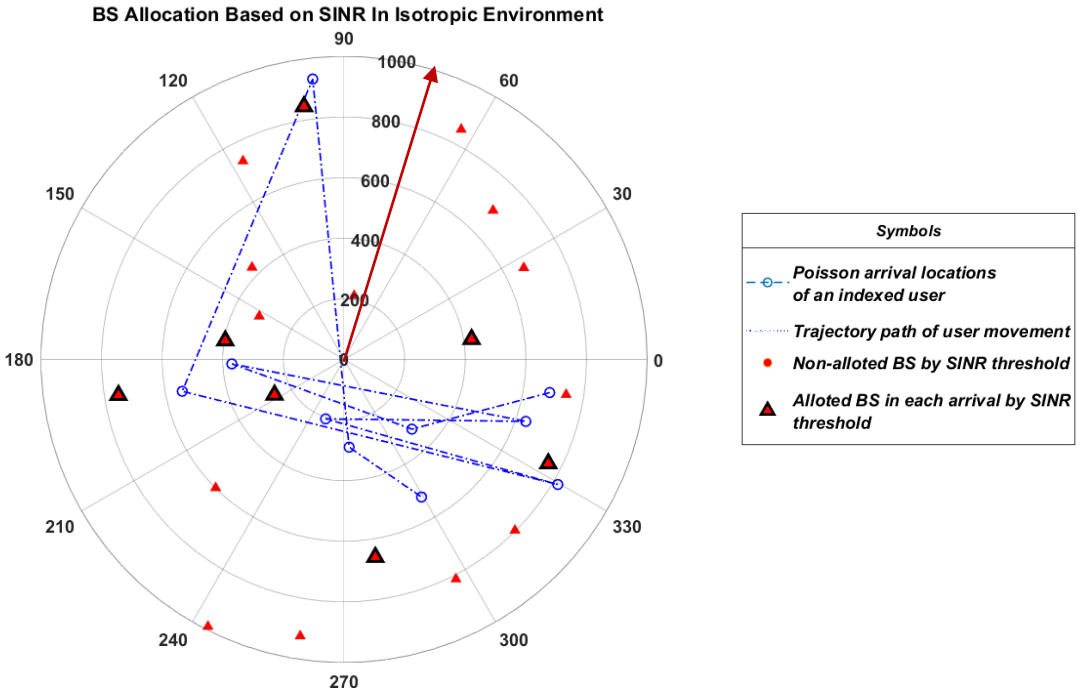

Fig 5.5. BS Allocation in isotropic network based on SINR threshold

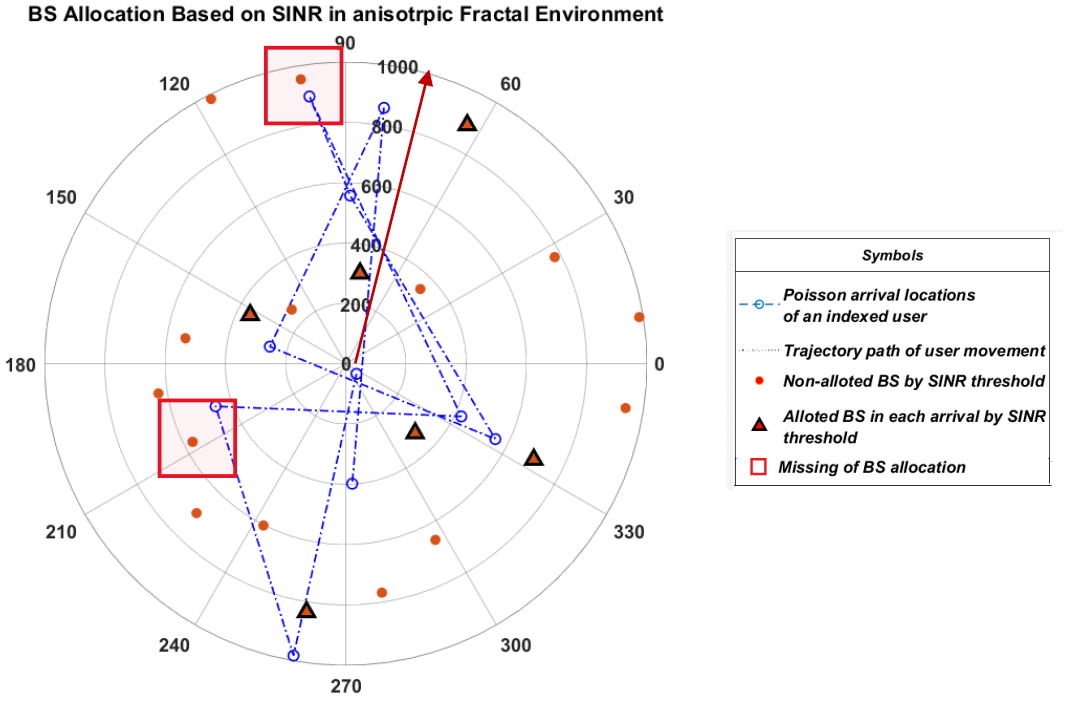

Fig 5.6. BS Allocation in anisotropic network based on SINR threshold

5.4.2. Results and Discussions

The performance of the fractal coverage is significantly impacted by the multi-directional fractal path loss exponents. To express the quality of network coverage, the coverage probability in terms of SINR and rate are measured considering the two factors SINR threshold (Γ) and achievable rate threshold (γ).

Figure 5.7 focuses on the probability of fractal coverage (in terms of SINR) to the SINR threshold (Γ). Horizontal observation shows that a gradual decrease of SINR coverage occurs on increasing the threshold value Γ. In the same figure, keeping the threshold Γ fixed, vertical interpretation reveals that the coverage probability in the mid-range of Γ decreases with increasing the value of σ i.e., the variance of the fractal exponent. More the value of σ, more fractal nature is injected into the network resulting in degradation of coverage performance. In this mid-region, the coverage performance is highest for the isotropic network ($\sigma = 0$), and lowest for the high fractal environment of $\sigma = 1$.

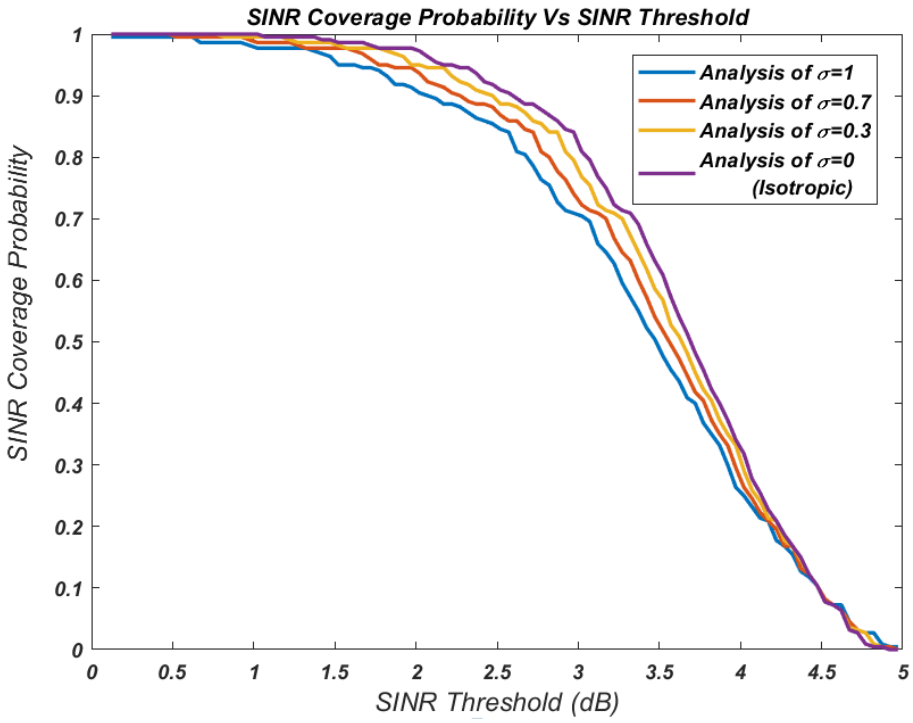

Fig 5.7. Probability of Coverage (SINR) Vs. Γ for discrete values of σ

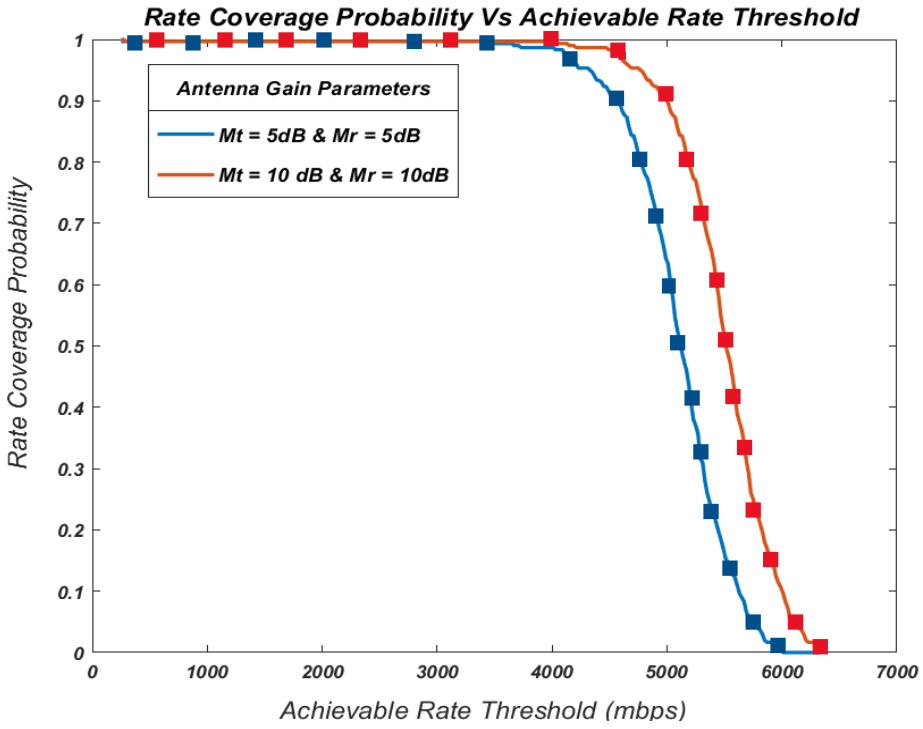

Fig 5.8. Probability of Coverage (Rate) Vs. γ for discrete values of Antenna Gain Parameters

Fig. 5.8 demonstrates the variation of coverage probability in terms of rate in accordance with the threshold rate (γ) for unique values of antenna lobe gains. If we increase the threshold rate γ, while keeping fixed antenna gain, the coverage probability in terms of rate decreases similar to that of the SINR coverage plot. From the figure, it is found that if the value of antenna main lobe gains of BS (M_t) and user (M_r) is decreased from 10 dB to 5 dB, the corresponding probabilities of rate coverage decrease due to the low beam strength of BS and user antenna.

The upcoming discussions will be made on the results obtained from the association probability of a fractal network. If a hypothetical BS (say BS_r, situating at a length r from the UE) is considered, the association probability shows the chance of having maximum SINR associated with it. Fig. 5.9.a shows the plot of association probability with the parameter distance from a user perspective. General observation shows that the association probability decreases

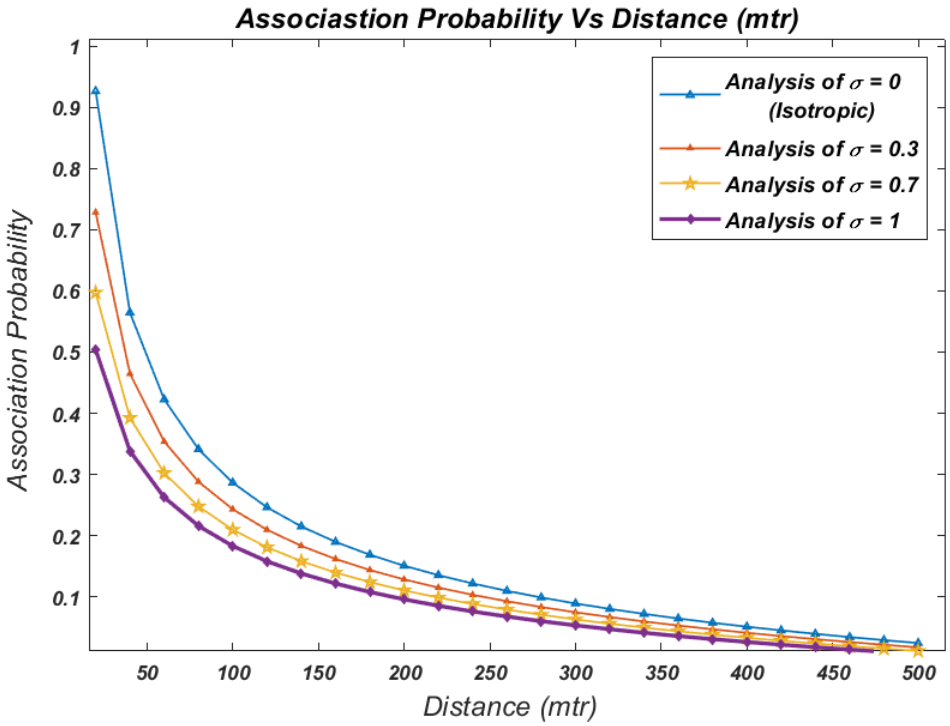

Fig 5.9.a Association Probability Vs. Distance for discrete values of path loss variance σ

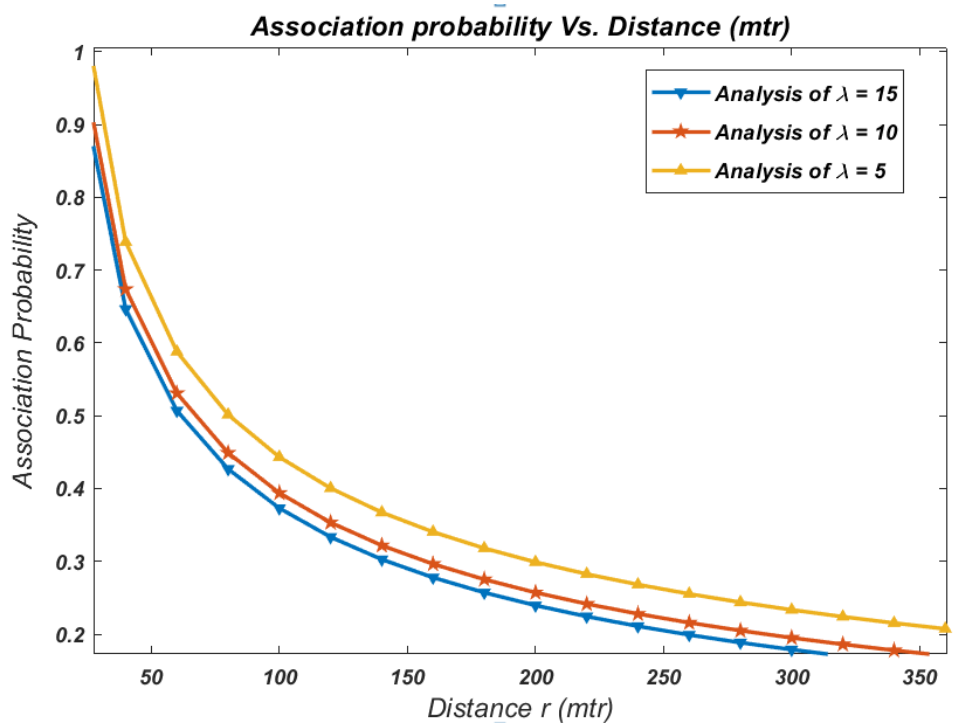

Fig 5.9.b Association Probability Vs. Distance for discrete values of BS density λ for σ=0.7

when distance is increased. It is obvious because, at higher distances, the chances of maximum SINR association with the considered BS becomes low. In the range of 100-300 meters, the anisotropic effect is prominent. The association probability is almost 1 in this region for the isotropic case, i.e., when $\sigma = 0$. It means the maximum SINR association is nearly assured with the desired BS_r. But increasing the variance value σ of path loss exponent will lower the probability of such an association incident even at a low distance. Rule of maximum SINR association is not guaranteed now for those BSs which are situated nearer to the user. The anisotropic effect almost vanishes in the higher distance range where all the characteristic curves have converged to a single point.

Fig. 5.9.b shows the same characteristics of association probability with distance but with different values of BS density λ. If non-uniform BS has been deployed by PPP, the density of BS can be varied by the parameter λ. From the graph, it can be interpreted that association probability is independent of BS density λ at very short distances (below 50 meters) and the value is almost 1 which means maximum SINR association occurs in this region. If we move further distance to the right of the plot, the association probability falls rapidly. The rate of fall is larger for high values of λ (λ=15) than for low values (λ=5).

Finally, the successful hand-off performance is compared for both isotropic and anisotropic environments in accordance with the SINR threshold (Fig. 5.10). Following the same SINR threshold algorithm used in the isotropic environment, the anisotropic medium, too, produces a similar shape of hand-off characteristics. The environmental characteristics are differentiated by the variance σ of the path loss exponent. For low SINR threshold ranges (0-1 dB), the successful hand-off rate is observed as almost 100 percent for all sets of σ i.e., it is independent of the nature of the environment. Between the ranges of 1-2 dB, the sets of curves can be easily distinguished by the rate of fall in accordance with the σ value. The rate

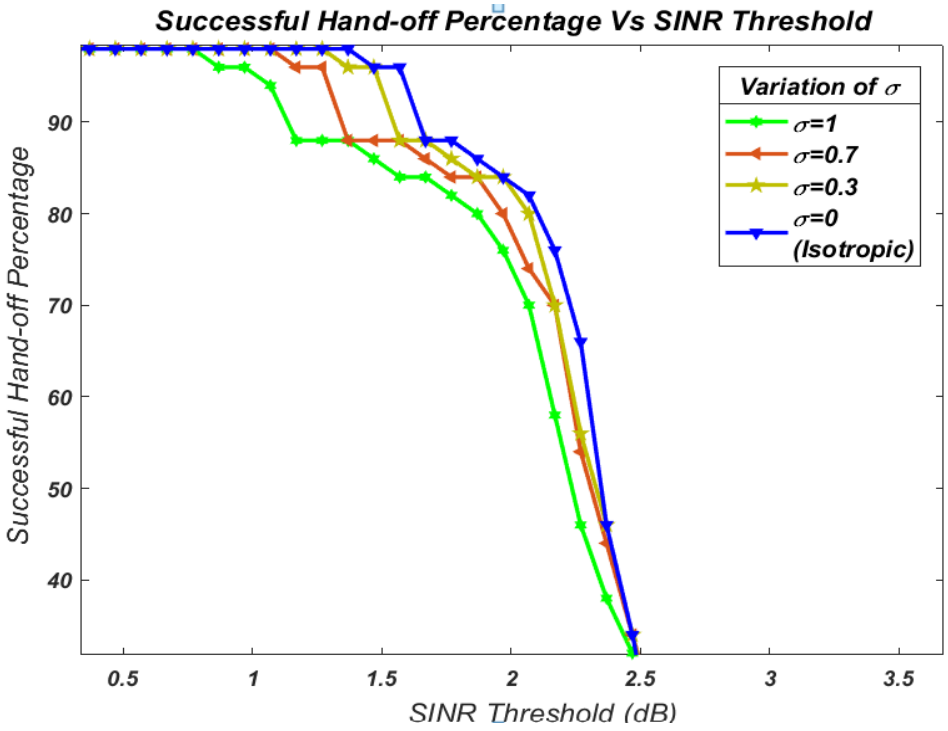

Fig 5.10. Handoff performance Vs. Γ for discrete values of variance σ And No. of Poisson arrival=50

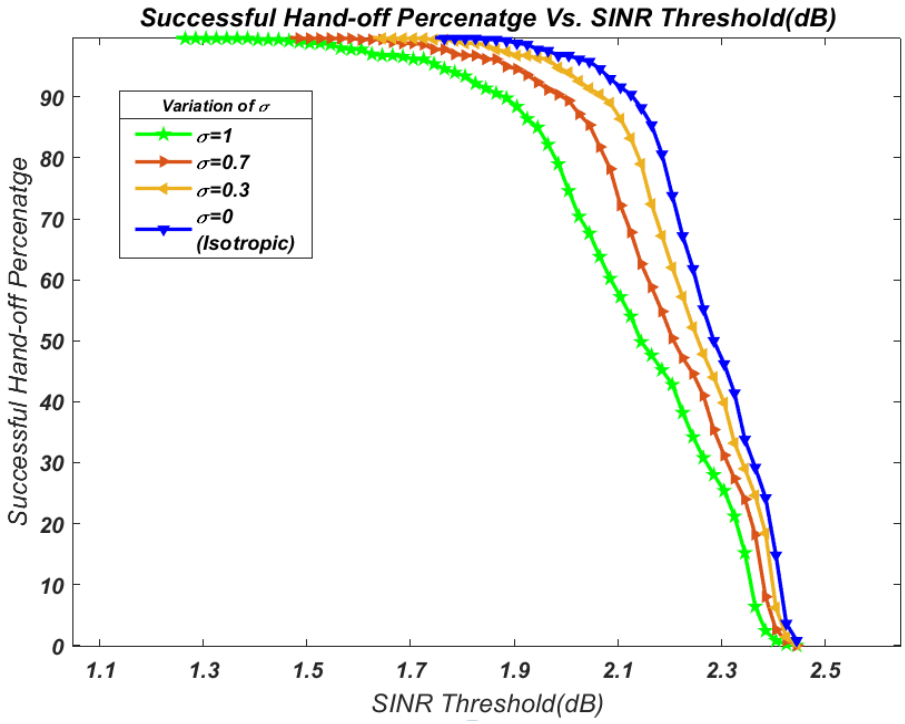

Fig 5.11. Handoff performance Vs. Γ for discrete values of variance σ and No. of Poisson arrival=500

of fall is highest for σ =1 (Anisotropic) and lowest for σ=0 (Isotropic). This degradation accounts for the lowering of hand-off performance which is the main challenge of designing or implementing the fractal network.

In Fig. 5.10, the gradual fall of the successful hand-off characteristics toward 0 convergence is not linear. It can be observed that the SINR threshold region 1-1.5 dB exhibits both uniform and non-uniform HO percentage values which indicates there will be suitable ranges of SINR threshold in practical scenarios. Modeling of a network in such SINR threshold ranges might show ambiguous performances. One way for obtaining smooth successful hand-off convergence is to increase the journey duration of user movement by increasing the number of Poisson arrival (N). In Fig. 5.11, stable convergence of successful hand-off characteristics is observed when the number of Poisson arrival is increased from 50 to 500. This can be explained below.

As successful HO percentage is the ratio between no. of successful Poisson arrival and Total No. of Poisson arrival, it readily gets stabilized when large no of sample points (arrivals) is taken in the denominator and the numerator variation is not large compared to the variation of denominator. Failed Poisson arrival cases do not vary as much because coverage of cells as well as the area of no-coverage zones (void region) is kept fixed throughout the experiment. Suppose, in a scenario, when no. of Poisson arrival is 10 and the avg. successful arrival varies between 6 to 8, the corresponding successful HO percentage fluctuation becomes 20 percent, but when no of Poisson arrival is increased to 100 and the avg. no. of successful arrival does not vary largely, say 60 to 70, shows only 10 percent fluctuation which is lesser than previous.

5.5 Chapter Summary

1. The non-homogeneous environment comprises multi-directional fractal path loss exponents that are distributed uniformly around a mean value μ with a variance σ.

2. The coverage probability in terms of SINR and rate decreases with the increase in the value of the SINR threshold (Γ) and achievable rate threshold (γ).

3. The Rule of maximum SINR association shows abrupt results in the anisotropic network while choosing the target BS by the SINR threshold metric. It is verified from the BS association characteristics that at a lesser distance, the probability of a BS becoming the serving BS for a user is much higher in a homogeneous environment than in a non-homogeneous environment.

4. The rate of successful hand-off percentage of a non-homogeneous environment falls with a greater slope in the SINR threshold range compared to an isotropic environment. The more the value of σ is, the more the degradation of hand-over performance.

5. The fluctuations in the successful hand-off characteristics are stabilized when the number of Poisson arrival of users is increased.

Chapter 6 Conclusion and Future Work

6.1 Conclusion

In this thesis, we have studied in detail the hand-off performance of 5G ultra-dense networks for enhancing the successful hand-off rate. The event hand-off takes place due to random user movement between two network cells. Thus, to relate the instantaneous user arrival locations (highly probabilistic), the knowledge of stochastic user distribution and their co-relation is required before analyzing the hand-off performance. The Poisson point Process, in short PPP, successfully serves the requirement of modeling the user distribution as well as user mobility framing. By proposing a recursive PPP algorithm in a test environment, the different aspects of the dynamic user characteristics are projected. With such characteristics, different user mobility models for a given network specification can be achieved by varying the parameter Poisson Inter-arrival time. A supporting example was shown in chapter 3, where the shifting of user mobility in terms of average velocity from a higher value (vehicular mode of transport) to a lower value (pedestrian walking) takes place when Poisson inter-arrival time is increased. Additionally, estimation of the dimension of an entire geographical region acts as one of the extended scopes of PPP.

The second part of our thesis works with the QoS improvement of hand-off in 5G distributed networks. The entire hand-off simulation and its analysis are implemented over the MATLAB testbed. Considering the nature of the propagating environment, the simulation analysis of hand-off is carried out in two phases, first in an isotropic environment and then in an anisotropic environment. Assuming user mobility to be supported by Poisson Point Process, the handover decision is evaluated on an algorithm based on a two-level threshold metric

checking on each user arrival instant.

In an isotropic path loss environment, to enhance handoff from a QoS perspective, the ratio of successful Poisson arrival counts to the total number of user arrival counts needs improvement (the total number of user arrival is fixed throughout the simulation). It can only be done by boosting the SINR for some of the poor user arrivals (previously discarded by the prefixed SINR threshold). To achieve this, the total interference power in the SINR is manipulated so that it can reduce in such a way that the modified SINR value of the user becomes high than the actual SINR (clustering method). It can now satisfy the hand-off threshold criteria for increased successful arrival counts. Numerical observation shows that the problem of poor QoS in the lower SINR threshold range of a 5G tier-1 FBS network is solved partially by the BS clustering method. The analysis also reveals that considering the minimum possible cluster radius cannot boost the range of successful handoff convergence beyond 0 dB. For this reason, we propose the implementation of a 2-tier FBS-MBS HetNet architecture. It exhibits stable performance in the entire SINR threshold range of successful handoff characteristics. The same behavior is also observed in the output of average throughput per BS of different network types. The throughput per BS decreases slightly (in the order of 1-2 Mbps) in tier-2 HetNet than in homogeneous networks. Also, user density, a function of the PPP parameter λ, is tuned in the average rate of BS, to see the dreadful impact on throughput performance.

As a non-homogeneous environment consists of different blocking elements of different dimensions, it follows a multi-directional propagating path loss model in which the success rate of hand-off performance is severely degraded. The conventional hand-off algorithm based on the SINR threshold metric behaves abruptly here. This can be accounted for by the decrease in association probability (maximum SINR association) of closely residing BS of a

user. The network coverage probability in terms of SINR and rate is measured against a suitable range of thresholds (both SINR and rate) for discrete values of path loss variance (σ). A high σ value ensures the injection of more fractality in a network that decreases the coverage probability of both the SINR and rate in the given range of thresholds. Finally, an initiative is taken to relate mobility with hand-offs for both homogeneous and non-homogeneous environments. It concludes that frequent hand-off fluctuations over the SINR threshold become stable when the number of Poisson arrival is increased.

6.2 Future Scope

1. Dynamic modulation of PPP on the account of user mobility in chapter 3 has a broad area to explore. Besides estimating different mobility models from the PPP characteristics, PPP can also be used to model and analysis of a real deterministic user movement pattern by varying the Poisson inter-arrival time non-uniformly.

2. The SINR threshold range (chapter 4) used in the hand-off algorithm is evaluated by taking the minimum and maximum from all the sets of SINR values of all users, achieved at all Poisson arrival locations. This significantly increases the time complexity (time to determine overall SINR set) as well as space complexity (Range of SINR threshold) of the simulation algorithm. In the future, an adaptive algorithm for finding the optimum SINR threshold of a system can be implemented to minimize both the time and space complexities in the decision stage.

3. In a non-homogeneous environment, the determination of the fractal exponent based on user arrival coordinates becomes the primary task of the hand-off sensing module that increases the network latency (chapter 5). In the future,

the incorporation of some of the fast linear or non-linear mathematical prediction models for predicting fractal exponent can be worked upon to minimize the network latency (by reducing the extra overhead of channel signaling).

4. An anisotropic environment (chapter 5) does not guarantee the association of the nearest BS to a user i.e., the rule of maximum SINR association fails sometimes. As a result, the corresponding Poisson arrivals are marked unsuccessful by the hand-off metrics. A futuristic solution of providing backup base stations for the failed cases can be implemented which will not only decrease the call dropping probability but also increase the success rate of hand-over.

5. The concept of non-homogeneity in chapter 5 is based on the segmentation of a region with different path loss exponents. Non-homogeneity can also be projected over the same region by segmenting it with different user densities (λ). The hand-off performance analysis of such environments is a good topic for future work.

6. Green communication is a crucial upcoming research area where SINR optimization can be utilized for power efficiency.

References

[1] M.A. Adedoyin, O.E. Falowo, “Combination of ultra-dense networks and other 5G enabling technologies: a survey”, IEEE Access (2020), https://doi.org/10.1109/ ACCESS.2020.2969980.

[2] Quang, R. V. Prasad, and I. Niemegeers, “A Survey on Hand-offs Lessons for 60 GHz Based,” IEEE Communications Surveys & Tutorials, vol. 14, no. 1, pp. 64–86, 2012H. Poor, An Introduction to
Signal Detection and Estimation. New York: Springer-Verlag, 1985, ch. 4.

[3] B. V. Quang, R. V. Prasad, and I. Niemegeers, “A Survey on Handoffs Lessons for 60 GHz Based,” IEEE Communications Surveys & Tutorials, vol. 14, no. 1, pp. 64–86, 2012. E. H. Miller, “A note on reflector arrays (Periodical style—Accepted for publication),” IEEE Trans. Antennas Propagat., to be published.

[4] 3GPP TS 36.331, “E-UTRA Radio Resource Control (RRC); Protocol specification (Release 9),” 2016.

[5] C. Çeken, S. Yarkand, H. Arslan, “Interference aware vertical handoff decision algorithm for quality of service support in wireless heterogeneous networks”, Comput. Networks. (2010).

[6] J. Chen, X. Ge, Q. Ni, “Coverage and handoff analysis of 5G fractal small cell networks”, IEEE Trans. Wirel. Commun. (2019), https://doi.org/10.1109/ TWC.2018.2890662.

[7] Di Gregorio, Lorenzo, “Latency in 5G Networks” on 1st Workshop on Mobile Systems Technology, May 22, 2015, Milan.

[8] X. Ge, Y. Qiu, J. Chen, et al., “Wireless fractal cellular networks,” IEEE Wireless Commun. Mag., vol. 23, no. 5, pp. 110–119, Oct. 2016

[9] M. N. Kulkarni, S. Singh, and J. G. Andrews, “Coverage and rate trends in dense urban mmWave cellular networks,” in IEEE GLOBECOM, Austin, TX, USA, Dec. 2014, pp. 3809–3814

[10] D. Xenakis, N. Passas, L. Merakos, C. Verikoukis, Handover decision for small cells: algorithms, lessons learned and simulation study, Comput. Netw. 100 (2016) 64–74, https://doi.org/10.1016/j.comnet.2015.11.003.

[11] Guidolin, I. Pappalardo, A. Zanella, and M. Zorzi, “ContextAware Handover Policies in HetNets,” IEEE Transactions on Wireless Communications, vol. 15, no. 3, pp. 1895–1906, 2016.

[12] H. Leem, J. Kim, D. K. Sung, Y. Yi, and B.-h. Kim, “A Novel Handover Scheme to Support Small-cell Users in a HetNet Environment,” in 2015 IEEE Wireless Comm. unications and Networking Conference (WCNC), 2015, pp. 1978–1983

[13] Z. Guohua, P. Legg, and G. Hui, “A network controlled handover mechanism and its optimization in LTE heterogeneous networks,” in IEEE Wireless Communications and Networking Conference, WCNC, 2013, pp. 1915–1919.

[14] Murtaza Cicioglu, “Performance analysis of handover management in 5G small cells” in Computer Standards & Interfaces 75 (2021) 103502

[15] Sun, Y., Feng, G., Qin, S., Liang, Y.-C. and Yum, P. T.-S. (2018) “The SMART handoff policy for millimeter-wave heterogeneous cellular networks”. IEEE Transactions on Mobile Computing, 17(6), pp. 1456- 1468.

[16] M. Mezzavilla, S. Goyal, S. Panwar, S. Rangan, and M. Zorzi, “An MDP Model for Optimal Handover Decisions in mmWave Cellular Networks,” in Networks and Communications (EuCNC), 2016 European Conference on. IEEE, 2016, pp. 100–105.

[17] Harpreet S. Dhillon, Radha Krishna Ganti, Franc¸ois Baccelli, and Jeffrey G. Andrews, Modeling and Analysis of K-Tier Downlink Heterogeneous Cellular Networks, IEEE JOURNAL ON SELECTED AREAS IN COMMUNICATIONS, VOL. 30, NO. 3, APRIL 2012

[18] X. Ge, X. Tian, Y. Qiu, et al., “Small Cell Networks with Fractal Coverage Characteristics,” IEEE Trans. Commun., vol. 66, no. 11, pp. 5457–5469, Nov. 2018

[19] Jiaqi Chen, Xiaohu Ge, and Qiang Ni, “Coverage and Handoff Analysis of 5G Fractal Small Cell Networks”, IEEE Transactions on Wireless Communications, Volume:18, Issue:2,February2019,
DOI:10.1109/TWC.2018.2890662.

[20] Nasıf Ekiz, Tara Salih, Sibel Küçüköner, and Kemal Fidanboylu “An Overview of Handoff Techniques in Cellular Networks” World Academy of Science, Engineering and Technology 6 2005

[21] P. Marichamy, S. Chakrabati and S. L. Maskara, “Overview of handoff schemes in cellular mobile networks and their comparative performance evaluation”, IEEE VTC’99,vol. 3, 1999, pp. 1486-1490.

[22] S. Choi and K. Sohraby, “Analysis of a Mobile Cellular Systems with Hand-off Priority and Hysteresis Control”, IEEE INFOCOM 2000, vol. 1, March 2000, pp. 217-224.

[23] “4G Mobile Network Architecture”, Kalle Ikkelä, Marko Myllynen, Juha Heinanen and Olli Martikainen Lappeenranta University of Technology, Lappeenranta, Finland

[24] Xavier Gelabert, Guohua Zhou, Peter Legg, “Mobility performance and suitability of macro cell power-off in LTE dense small cell HetNets” IEEE 18th International Workshop on Computer Aided Modeling and Design of Communication Links and Networks (CAMAD), pp. 99-103, 2013.

[25] Aleksi Peltonen, Ralf Sasse, David Basin “A Comprehensive Formal Analysis of 5G Handover” WiSec ’21, June 28–July 2, 2021, Abu Dhabi, United Arab Emirates https://doi.org/10.1145/3448300.3467823

[**26**] Ludwig, J.A., Reynolds, J.F.: Statistical Ecology: a Primer on Methods and Computing. John Wiley & Sons, New York (1988)

[27] Parzen, E.: Stochastic Processes. Holden-Day, San Francisco (1962). (OCoLC)565202779, ISBN :0816266646 9780816266647

[28] Adrian Baddeley, “Spatial Point Processes and their Applications” School of Mathematics & Statistics, University of Western Australia Nedlands WA 6009, Australia.

[30] Diggle, P.J. Statistical Analysis of Spatial Point Patterns. Second edition, ,Arnold, London (2003)

[29] Kingman, J.F.C.: Poisson Processes. Oxford University Press, Oxford (1993), ISBN: 9780198536932

[31] T. Camp, J. Boleng and V. Davies, “A survey of mobility models for ad hoc network research,” Wireless Commun. Mobile Comput.łSpecial Issue Mobile Ad Hoc Netw., Res., Trends, Appl., vol. 2, no. 5, pp. 483–502, Aug. 2002.
[32] C. Bettstetter, H. Hartenstein and X. P. Costa, “Security and performance challenges for user-centric wireless networking,” Wireless Networks, vol. 10, no. 5, pp. 555–567, Sept. 2004

[33] X. Wang, X. Lei, P. Fan and R. Q. Hu, “Cost analysis of movementbased location management in pcs networks: an embedded markov chain approach,” IEEE Trans. Veh. Technol., vol. 63, no. 4, pp. 1886–1902, May 2014

[34] C. Song, T. Koren, P. Wang and A. L. Barabsi, “Modeling the scaling properties of human mobility,” Nature Physics, vol. 6, pp. 818–823, 2010

[35] User Mobility Evaluation for 5G Small Cell Networks Based on Individual Mobility Model; iaohu Ge 1 , Junliang Ye 1 , Yang Yang 2 , 3 , Qiang Li 1 IEEE JOURNAL ON SELECTED AREAS IN COMMUNICATIONS, VOL. XX, NO. Y, MONTH 2016

[**36**] ——, “Path loss models for 5G millimeter wave propagation channels in urban microcells,” in IEEE G36obal Communications Conference (GLOBECOM), Dec. 2013, pp. 3948–3953.

[37] S. Sun et al.,” Propagation Path Loss Models for 5G Urban Micro- and Macro-Cellular Scenarios,” in 2016 IEEE 83rd Vehicular Technology Conference (VTC2016-Spring), May 2016

[38] V.S. Abhayawardhana, I.J. Wassel, D. Crosby, M.P. Sellers, M.G. Brown (2005) 61st IEEE Technology Conference

[39] Yazan A Alqudah, “On the Performance of Cost 231 Walfish Ikegami Model in Deployed 3.5 GHz Network”, International Conference on Technological Advances in Electrical, Electronics and Computer Engineering (TAEECE).

[40] Hucheng Wang, Shanzhi Chen, Ming Ai, and Hui Xu, “Localized Mobility Management for 5G Ultra Dense Network”

[41] R. Balakrishnan and I. F. Akyildiz, “Local mobility anchoring for seamless handover in coordinated small cells,” in Proc. IEEE Global Commun. Conf., Atlanta, GA, USA, 2013, pp. 4489–4494.

[42] Vikas Paliwal, I. lambadaris, “Cell Search Procedures in LTE Systems”, Published in 2012, Department of Systems and Computer Engineering.

[43] Thiri Wai, Htay Htay Thaung, “Shortest-Path Finding System using Dijkstra’s Algorithm”, University of Computer Studies, Maubin, Myanmar

[**44**] Y. S. Meng, Y. H. Lee and B. C. Ng, “Empirical Near Ground Path Loss Modeling in a Forest at VHF and UHF Bands,” IEEE Trans. Antennas Propag., vol. 57, no. 5, pp. 1461–1468, May 2009

[45] T. Bai, R. Vaze and R. W. Heath, “Analysis of Blockage Effects on Urban Cellular Networks,” IEEE Trans. Wireless Commun., vol. 13, no. 9, pp. 5070–5083, Sept. 2014

[46] L. Xiang, X. Ge , C.-X. Wang, et al., “Energy Efficiency Evaluation of Cellular Networks Based on Spatial Distributions of Traffic Load and Power Consumption,” IEEE Trans. Wireless Commun., vol. 12, no. 3, pp. 961–973, Mar. 2013

[47] R. A. Dwyer. “A faster divide-and-conquer algorithm for constructing delaunay triangulations”. Algorithmica, 2:137–151, 1987.

[48] 3GPP, “TR 36.814, Further advancements for E-UTRA physical layer aspects,” Mar. 2017

[49] M. N. Kulkarni, S. Singh, and J. G. Andrews, “Coverage and rate trends in dense urban mmWave cellular networks,” in IEEE GLOBECOM, Austin, TX, USA, Dec. 2014, pp. 3809–3814

[50] J. Chen, F. Bin, X. Ge, et al., “A dual-directional path-loss model in 5G wireless fractal small cell networks,” in IEEE ICC, Paris, France, May 2017, pp. 1–6

[51] 3GPP, “TR 38.900, Technical Specification Group Radio Access Network; Study on channel model for frequency spectrum above 6 GHz ,” Jul. 2017